En-échelon Rifting and Origin of the Volcanism in the Comoros

Pierre Boymond, Nathalie Feuillet, Isabelle Thinon, Luc Scholtes, Sébastien Zaragosi, Sylvie Leroy, Anne Lemoine

Geochemistry, Geophysics, Geosystems®

RESEARCH ARTICLE
10.1029/2024GC011576

En-échelon Rifting and Origin of the Volcanism in the Comoros

P. Boymond[1], N. Feuillet[1], I. Thinon[2], L. Scholtès[3], S. Zaragosi[4], S. Leroy[5], and A. Lemoine[2]

[1]Institut de Physique du Globe de Paris (IPGP), Université Paris Cité, Paris, France, [2]Bureau de Recherches Géologiques et Minières (BRGM), Orléans, France, [3]Laboratoire Magmas et Volcans (LMV), Université Clermont Auvergne, CNRS, IRD, OPGC, Clermont-Ferrand, France, [4]CNRS, EPOC, UPHE, UMR 5805, Université de Bordeaux, Pessac, France, [5]CNRS-INSU, Institut de Sciences de la Terre de Paris, ISTeP, Sorbonne Université, Paris, France

Key Points:

- Characterization of NW-SE-striking active volcanic and tectonic structures in the Comoros archipelago from high resolution marine data
- Evidence for late Quaternary rifting episodes in the Mwezi and N'Droundé submarine volcanic provinces within a N40°E regional extension
- *En-échelon* rifts compatible with right lateral shear in a transfer zone between the offshore East African rift system and Malagasy rift

Supporting Information:

Supporting Information may be found in the online version of this article.

Correspondence to:

P. Boymond,
boymond@ipgp.fr

Citation:

Boymond, P., Feuillet, N., Thinon, I., Scholtès, L., Zaragosi, S., Leroy, S., & Lemoine, A. (2025). *En-échelon* rifting and origin of the volcanism in the Comoros. *Geochemistry, Geophysics, Geosystems*, *26*, e2024GC011576. https://doi.org/10.1029/2024GC011576

Received 23 APR 2024
Accepted 16 DEC 2024

Abstract Two volcanic provinces have been recently discovered during the SISMAORE oceanographic cruise in the Comoros archipelago in the North Mozambique Channel between Madagascar and East Africa: N'Droundé, along the North-eastern insular slopes of Grande Comores Island and Mwezi, in the abyssal plain, north-east of Mayotte and Anjouan islands. By combining bathymetry and backscatter data, high-resolution seismic reflection and sub-bottom profiles, we have identified and mapped various tectonic (faults, forced folds) and volcanic structures (lava flows, edifices, sills, dykes) at several spatial scales on the seabed and in cross-section within the sedimentary cover. We have characterized the volcano-tectonic structures (geometry, segmentation, and kinematics) to better understand the link (geometry, chronology) between tectonic and volcanic processes. We show that volcanic and tectonic features are controlled by tectonic processes and vice-versa. Ridges, volcanic cones and lava flows are set up along fissures and dikes during main rifting events to accommodate a N40°E regional extension within an E-W right lateral shear transfer zone. The volcano tectonic features are Plio-Pleistocene. This transfer zone lies between the offshore branch of the East African rift system and Malagasy grabens and may have formed when the East African rifts propagated offshore. We evidence a major rifting episode in the last Ma. The estimated volume and flux of extruded lavas show that the volcanism of the Comoros could be related to shallow tectonic processes.

1. Introduction

As in many regions of the world, the origin of intraplate volcanism in the Comoros archipelago (North Mozambique channel, between Madagascar and East Africa) is poorly understood and opposing models have been proposed (Deep mantle plumes vs. surface processes). Interest in the submarine domain of this area was renewed after the largest submarine eruption ever documented occurred off Mayotte in the Comoros archipelago and gave birth to a new volcano (Fani Maore) in 2018 (Feuillet et al., 2021). At least 6.5 km^3 of basanitic magma was extruded in a few months from deep mantle reservoirs (Berthod et al., 2021; Feuillet et al., 2021; Lemoine et al., 2020), a volume larger than the recent massive basaltic 2018 Hawaii and 2020 Iceland eruption (Dietterich et al., 2021). The Fani Maore eruption came as a surprise in a region where no other historical eruptions have been documented, with the exception of Karthala on the island of Grande Comores. Several hypotheses have been put forward to explain the origin of the Comoros archipelago: Emerick and Duncan (1982) inferred that it was part of a hotspot track: Nougier et al. (1986) proposed that it resulted from the reactivation of old late-Triassic and early-Jurassic fractures zones inherited from the opening of the North Mozambique Channel (Nougier et al., 1986) and more recently, Michon (2016) suggested that it belongs to the East African Rift System (EARS, Michon, 2016). Since the discovery of the new volcano, a large amount of geological and geophysical data has been collected during several campaigns at sea (MAYOBS, Rinnert et al., 2019, GEOFLAMME, Rinnert et al., 2021; SISMAORE, Thinon et al., 2020). Those data provided evidence of Paleogene to Quaternary volcanic activity in the entire archipelago (Feuillet et al., 2021; Masquelet et al., 2022, 2023; Rusquet et al., 2023; Thinon et al., 2022) that contributed to the edification of the volcanic islands during several volcanic phases, which are coeval to those in the EARS and in Madagascar (Michon et al., 2022). Chauvel et al. (2024) showed that the volcanic products (basanite, tephri-phonolites and phonolites) emitted off Mayotte during the 2018 eruption (and earlier in the region) came from the melting of a carbonated mantle source common to the African rift. These recent discoveries contradict the oldest hotspot model and suggest a relationship between the offshore branch of the EARS, the Comoros archipelago and the rifts in Madagascar (Feuillet et al., 2021; Michon, 2016; Michon et al., 2022). Such interactions share similarities with other rift-to-rift interactions observed in the EARS (such as the Rukwa and

Mweru-Wantipa rifts, Ajala et al., 2024; Kolawole & Ajala, 2024) but at greater distances. However, the way in which these main systems interact with each other is not yet understood as we are missing high resolution multi-scale characterization of the volcano-tectonic structures in the Comoros archipelago. Block models of the Global Navigation Satellite System (GNSS) showed that several lithospheric plates exist in this region (Victoria, Nubia, Lwandle, Rovuma, Somalia, Calais et al., 2006; Saria et al., 2014; Stamps et al., 2018, 2021, inset of Figure 1a). The nature, location and kinematic of the plate boundaries are however still unprecise in the Mozambique channel although several deformation models have recently been proposed in the literature: (a) from the identification of various tectonic structures (Riedel shear, *en-échelon* tension cracks and folds), Famin et al. (2020) inferred that the Comoros archipelago lies on an immature right-lateral transpressional boundary between Lwandle and Somalia plate; (b) Stamps et al. (2021), based on GNSS models, rather concluded that this boundary is a 1,000 km wide diffuse zone of deformation including the archipelago; (c) Thinon et al. (2022), from spatial distribution and orientation of vast volcanic provinces along the Comoros archipelago (see details later in part 2), inferred the existence of a dextral shear corridor along an immature plate boundary (dashed zone in the inset of Figure 1a); (d) Feuillet et al. (2021) proposed an alternative model and inferred an E-W striking right-lateral transtensional transfer zone between the EARS offshore branch and the Malagasy rift (i.e., Aloatra-Ankay grabens, Ambre Massif, Figure 1b). The extensional and oblique structures (NNW-SSE-striking step overs and E-W diffuse relay zones), accommodating the deformation in this transfer zone, guide the emplacement of volcanic products and constitute high-permeability zones where reservoirs and magma plumbing systems could develop. This later hypothesis implies that the volcanism in the Comoros could be in part controlled by extensional strain, conserved along an 800 km-long transfer zone between main rift segments of the EARS.

Transfer zones between rift segments were mainly identified and documented in the continental domain along the EARS (i.e., Kolawole & Ajala, 2024; Kolawole et al., 2021; Nelson et al., 1992, and reference therein) and studied via analog sand box models (Acocella et al., 2005; Corti, 2012; Corti et al., 2007; De Souza Rodrigues et al., 2023). They are a wide zone of diffuse complex deformation of various styles and geometries (extensional, strike -slip oblique) within overlapping or underlapping rift segments (Corti, 2012; Kolawole et al., 2021 and reference therein). In the offshore domain, oceanic ridges interact each-others via transform fault systems. Analog models showed that their nature and geometry depend on several parameters (thickness and basal topography of the lithosphere, presence of inherited structures and other weakness zones in the lithosphere). However, they are still poorly documented in the offshore domain because we often miss high resolution marine data to describe the associated volcano-tectonic structures at several spatio-temporal scales.

Here we used a new marine data set acquired in 2021 during the SISMAORE cruise (Thinon et al., 2022) to document, with an unprecedented resolution, the volcano-tectonic processes in the Comoros archipelago and particularly in two vast volcanic provinces (N'Droundé and Mwezi), recently unveiled (Thinon et al., 2022). By combining bathymetry and backscatter data, high-resolution seismic reflection and sub-bottom profiler data, we first identified and mapped various tectonic (faults, forced folds) and volcanic structures (Ridges, lava flows, volcanic cones, sills, dykes) at various spatial scales (from meters to hundred kilometers) on the seabed and in seismic sections within the sedimentary cover. We defined major volcano-tectonic structures. We then analyzed their distribution, geometry, segmentation, kinematics and evolution to determine the style and mechanism of the active deformation. The orientation of the regional stress field is deduced from a mechanical model of major dyke systems. Finally, we discuss the volcano-tectonic processes at play and the origin of the Comorian volcanism as well as the implications for the kinematics of the EARS system and the geodynamics in the area.

2. Geological Setting and Main Submarine Structures in the Comoros Archipelago

The Comoros archipelago is located in the North Mozambique Channel. This Channel opened to accommodate the East Gondwana breakup between the late-Triassic and early-Jurassic (Gibbons et al., 2013; Lawyer et al., 1991). The archipelago is composed of four main volcanic islands (Grande-Comore, Mohéli, Anjouan and Mayotte) and submerged features (Zélée-Geyser banks, the Vailheu seamount, and the Jumelles, Domoni, Chistwani, Safari and East Mayotte volcanic chains, e.g., Feuillet et al., 2021; Thinon et al., 2022; Tzevahirtzian et al., 2021) which lie in the abyssal plain, straddling the Somali basin and the Comoros basin (Figure 2). Volcanic activity initiated 28 Ma ago in Mayotte and extended eastward to form Anjouan and Moheli islands 9 Ma ago (Masquelet et al., 2023). The island of Grande Comores, where lies the active Karthala volcano, is the youngest island of the archipelago (~2 Ma, Masquelet et al., 2023). Volcanic activity is still present today, as evidenced by the occurrence of several eruptions since the early 18th century at the Karthala volcano (Bachèlery, 1995;

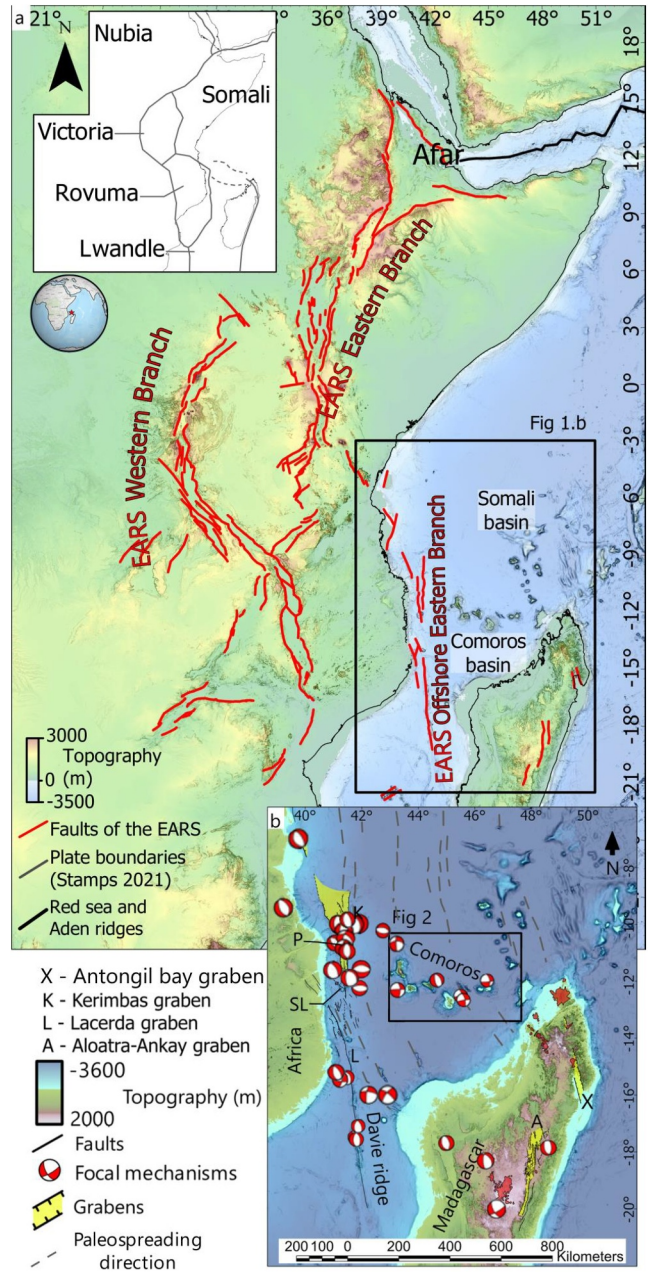

Figure 1. The East African Rift System (EARS): Tectonic and geodynamic context of the Comoros Archipelago (Northern Mozambique Channel between the Africa and Madagascar). Shaded topography and bathymetry from (@GEBCO 2022, https://doi.org/10.5285/e0f0bb80-ab44-2739-e053-6c86abc0289c). (a) The major regional Cenozoic structures in the area (red and lines) with names are redrawn and simplified from Michon et al. (2022), Klimke and Franke (2016), Courgeon et al. (2018), Mougenot et al. (1986), Franke et al. (2015), Bésairie (1957), Piqué et al. (1999), and Kusky et al. (2010)) and references therein. Inset: Major lithospheric plates in the area from Stamps et al. (2021). Dashed lines suggest a diffuse plate boundary (Stamps et al., 2021) and highlight the corridor of volcano-tectonic deformation as defined by Thinon et al. (2022). (b). Close up view of the regional fault systems focusing on the Volcanic Comoros archipelago. Structures and references as in (a) but presented in more detail. Main Cenozoic basins of the offshore branch of the EARS (Kerimbas -K-and Lacerda -L grabens) and in Madagascar (Aloatra-Ankai (A) and Antongil Bay grabens (X)) are indicated by yellow patches. Focal mechanisms from the CMT database (Ekström et al., 2012) redrawn from Lemoine et al. (2020) in red. The Cenozoic volcanic systems and seamounts are indicated with red patches of seamounts (St-Lazare (SL) and Paisley (P)). Dashed N-S black line: Paleospreading direction within the seafloor fabric from Davis et al. (2016). North of the Comoros archipelago, the crust is oceanic (Masquelet et al., 2023 and reference therein) and Jurassic (between 150 and 120 Ma, Davis et al., 2016).

Bachèlery, Morin, et al., 2016; M. Krafft, 1982) and recently off Mayotte. Pleistocene volcanic activity has been documented in all islands of the archipelago (Rusquet et al., 2025), along with younger volcanic products of Holocene age in Grande-Comores (La Grille volcano, Bachèlery, Lenat, et al., 2016) and in Anjouan (Quidelleur et al., 2022). In Mayotte, before the eruption, the only evidence of Holocene activity was a 7 ka-yr old-tephra layer found by coring in the lagoon (Zinke et al., 2003).

The "background" (i.e., in the absence of volcanic unrest or eruption) seismicity rate is low in the area. Only a few focal mechanisms were calculated for the main magnitude class 5 earthquakes (Figure 1b). They are compatible with strike-slip and normal faulting and are distributed in an E-W corridor along the Comoros archipelago (Bertil & Regnoult, 1998; Bertil et al., 2022; Lemoine et al., 2020).

In the offshore domain, the high-resolution marine data of several geophysical marine cruises (BATHYMAY, Audru et al., 2006; SHOM (Shom, 2016. Projet Homonim http://dx.doi.org/10.17183/MNT_MAY100m_HOMONIM_WGS84), MAYOBS, Rinnert et al., 2019, SISMAORE, Thinon et al., 2020) revealed the existence of various volcanic and tectonic structures on the insular shelf of Mayotte (Audru et al., 2006; Feuillet et al., 2021) and in the entire archipelago (Thinon et al., 2022; Tzevahirtzian et al., 2021). East of Mayotte, these volcanic structures compose an E-W to N140°E-striking volcanic ridge that results from an NE-SW regional extension (Feuillet et al., 2021). Long and narrow volcanic chains were documented in between the main islands of the archipelago (The N140°E Safari, the N70°E Chistwani, and the N160°E Domoni ridges) along with vast volcanic provinces in the Somali basin north of the archipelago: (a) N'Droundé, along the north-eastern island slopes of Grande Comores, and (b) Mwezi, in the abyssal plain, north-east of Mayotte and Anjouan (Thinon et al., 2022; Figure 2). The Mwezi province is 100 km -long and 60 km-wide and lies between 3,400 and 3,200 m below sea level (BSL, Figures 3a and 3b). It is located in the prolongation of the Jumelles volcanic chains and is elongated in the N130°E direction. The N'Droundé province (Figures 4a and 4b) extends over a 40-km-wide and 100-km-long area. It is composed of three NNW-SSE-striking volcanic chains lying between a depth of 735 and 3,400 m BSL. The westernmost chain emplaced on the northern slope of Grande Comore Island. Others are in the abyssal plain between a depth of 3,100 and 3,400 m BSL. Thinon et al. (2022) identified various types of volcanic edifices (cones, ridges, lava flows) and tectonic structures (faults, dome-shaped forced folds) in both provinces (see descriptions later in the text). Some are young, as attested by the K-Ar dating of a fresh rich-gas basaltic rock sample dredged on the flank of one of the edifices in the Mwezi volcanic province (~200 ka, Rusquet et al., 2025) or along the flanks of the Jumelles volcanic chains (between ~200 ka and 1.4 Ma, Berthod et al., 2021; Rusquet et al., 2025; Thinon et al., 2020, 2022; Figure 2).

3. Data, Processing, and Methodology

We used a part of the SISMAORE oceanographic cruise data set acquired in the Mwezi and N'Droundé provinces. The cruise (December 2020 to February 2021) onboard the Research Vessel Pourquoi Pas (Thinon et al., 2020) acquired about 80,000 km^2 of multibeam bathymetry and backscatter data with the vessel mounted Multibeam Echosounder System (MBES RESON 7150 at 12 or 24 kHz) in the North Mozambique Channel abyssal plain around the Comoros archipelago. In addition, 10,000 km of sub-bottom profiler (SBP) data and 6,730 km of 48-channel seismic reflection profiles were acquired simultaneously along the same navigation lines.

3.1. Bathymetry and Backscatter

We carried out a detailed analysis of the seabed by jointly analyzing bathymetric digital elevation models (DEM) and backscatter mosaics provided by Thinon et al. (2022) with a resolution of 30 m (Figures 3 and 4; Figure S1-2 in Supporting Information S1).

Although the backscatter signature (intensity of the retrodiffusion) can be influenced by the topographic slope of the seafloor (Urick, 1983), it provides information on both the texture (roughness) and potential nature of the seafloor: Stronger intensities (colors: white to light gray) indicate a hard bottom, like volcanic rocks, while weaker intensities (colors: dark gray to black) indicate a soft bottom, like loose sediments (Augustin, 1997; Augustin et al., 1996; Dugelay et al., 1996; Lurton, 2002). For a systematic and homogeneous interpretation of the backscatter map, we defined five facies in our study areas (Table S2 –1 in Supporting Information S1).

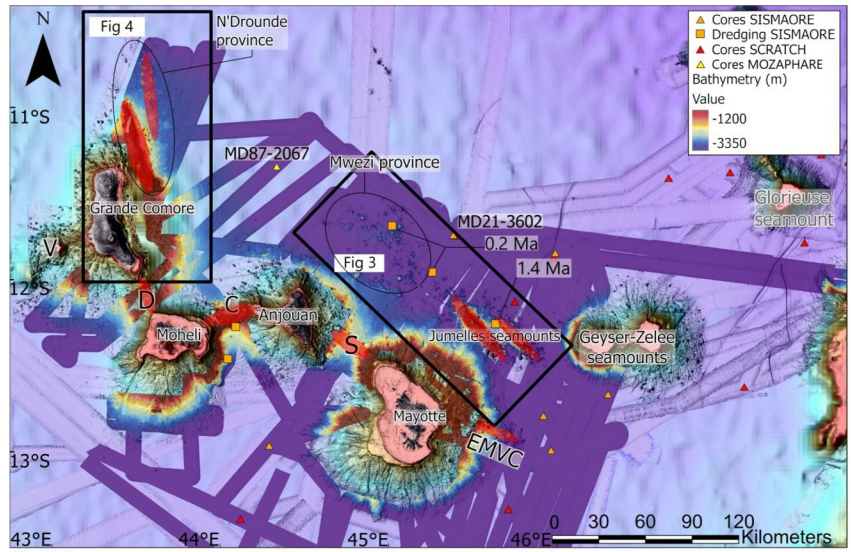

Figure 2. Topography, bathymetry and main physiographic features along the Comoros archipelagos. Bathymetry with shaded slope from SISMAORE campaign superimposed on the bathymetry SHOM-2022 compilation (lighter colors). V: Vailheu mount, D, C, S: Domoni, Chistwani and Safari chains, respectively, Thinon et al., 2022), EMVC (East Mayotte Volcanic Chain (Feuillet et al., 2021): Orange triangle and squares: SISMAORE cores and dredges, respectively, red triangle SCRATCH core (Berthod et al., 2021), yellow triangle MOZAPHARE core (Lancelot, 1996). The black contoured rectangular boxes indicate the extent of Figure 3 (Mwezi area) and Figure 4 (N'Droundé area).

Bathymetric maps with slope values (Figures 3a and 4a), topographic profiles and backscatter facies were used to identify and measure various volcanic and tectonic structures (Figures 3 and 4). The data set and interpretation were gathered in a GIS software (ArcGIS software, Environmental Systems Research Institute (ESRI) (2012). ArcGIS Release 10.2.1.)

3.2. 48-Channels Seismic and Sub-Bottom Profiler Data

We interpreted 26 SISMAORE 2D 48-Channel seismic reflection profiles (10 knots velocity, two guns, details for acquisition parameters are provided in Thinon et al. (2020, 2022), see locations and uninterpreted profiles in Supplementary 3 in Supporting Information S1). We used the post-stack time migrated seismic profiles (constant-velocity of 1,500 $m.s^{-1}$) with vertical and horizontal resolutions of about 5–10 m (signal thickness) and 12.5 m (inter-CDP distance), respectively. The signal penetrates depths of about 3 s Two Way Travel Time (s. TWTT) below the seafloor (i.e., ~4 km with the average velocity 2,500 $m.s^{-1}$ from Masquelet et al. (2022)). Most of the profiles are parallel and NW-SE oriented. They are crossed by a few EW-striking profiles, allowing correlations between them.

At the location of the 48-channel seismic lines, we also interpreted the Sub-Bottom profiler data (SBP; see locations and uninterpreted profiles in Supplementary 4 in Supporting Information S1), which provide a 2D very-high-resolution image (5 m in. horizontal and 25–30 cm in vertical) of the subsurface until 0.1 s TWTT below the seafloor (i.e., up to 85 m in using an arbitrary velocity 1,700 $m.s^{-1}$).

The seismic interpretation was performed using the IHS Kingdom software®. The main seismic unconformities and specific seismic reflectors in the 48-channel seismic and SBP were correlated from one profile to another. The identification of seismic facies and seismic units is based on the seismic stratigraphic principles from Mitchum et al. (1977) and is presented in Supplementary 5 in Supporting Information S1.

3.3. Age of the Seismic Reflections and Units From Coring Data

The ages of the major seismic horizons were estimated by using the sedimentation rates available from the sediment cores MD96-2067 (21.5 m-long, MOZAPHARE cruise, Lancelot, 1996) and MD21-3602 (32 m-long,

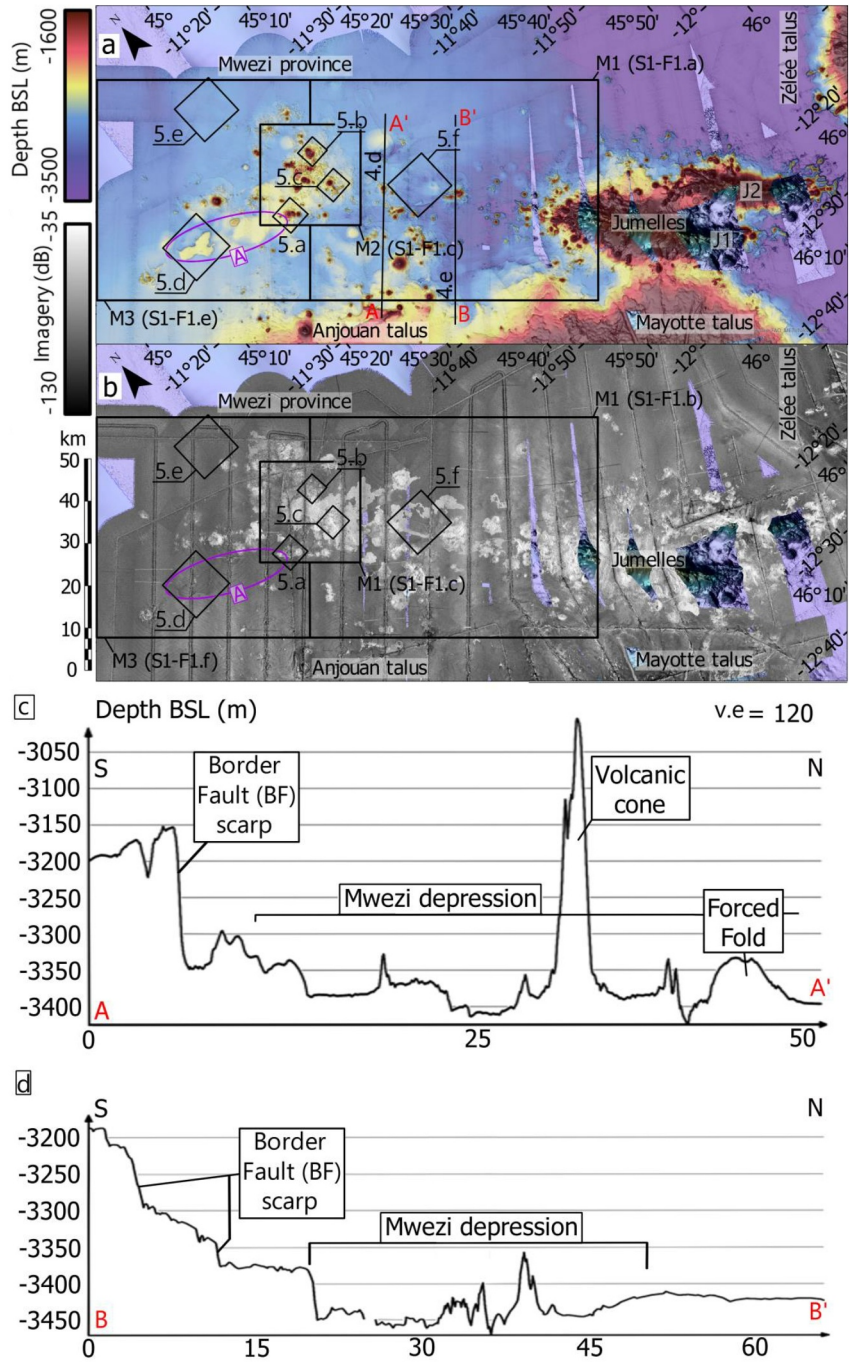

Figure 3. Bathymetric and backscatter maps in the Mwezi area (a, b). Black rectangles: subareas identified in each of these provinces are indicated: from west to east M1, M2, M3 in Mwezi. Red lines: locations of the topographic profiles A-A′ and B-B′ presented in (c) and (d). Black boxes: location of the bathymetric and backscatter close-up views presented in Figure 5. Topographic profiles A-A′ (c) and B-B′ (d) and main topographic features across the Mwezi (a, b) provinces.

SCRATCH cruise, Berthod et al., 2021). Those rates, determined by Oxygen isotopic stratigraphy, are ~5.4 and 3.1 cm/ka for the hemipelagic section in the cores MD87-2067 and MD21-3602 over the last 200 and 1,000 ka, respectively (see Figure S6-1 in Supporting Information S1 for details). By correlating the main sedimentary units observed in the cores to the main seismic horizons observed in the sub-bottom profiler data, we proposed an age for each reflector (Supplement 6 in Supporting Information S1).

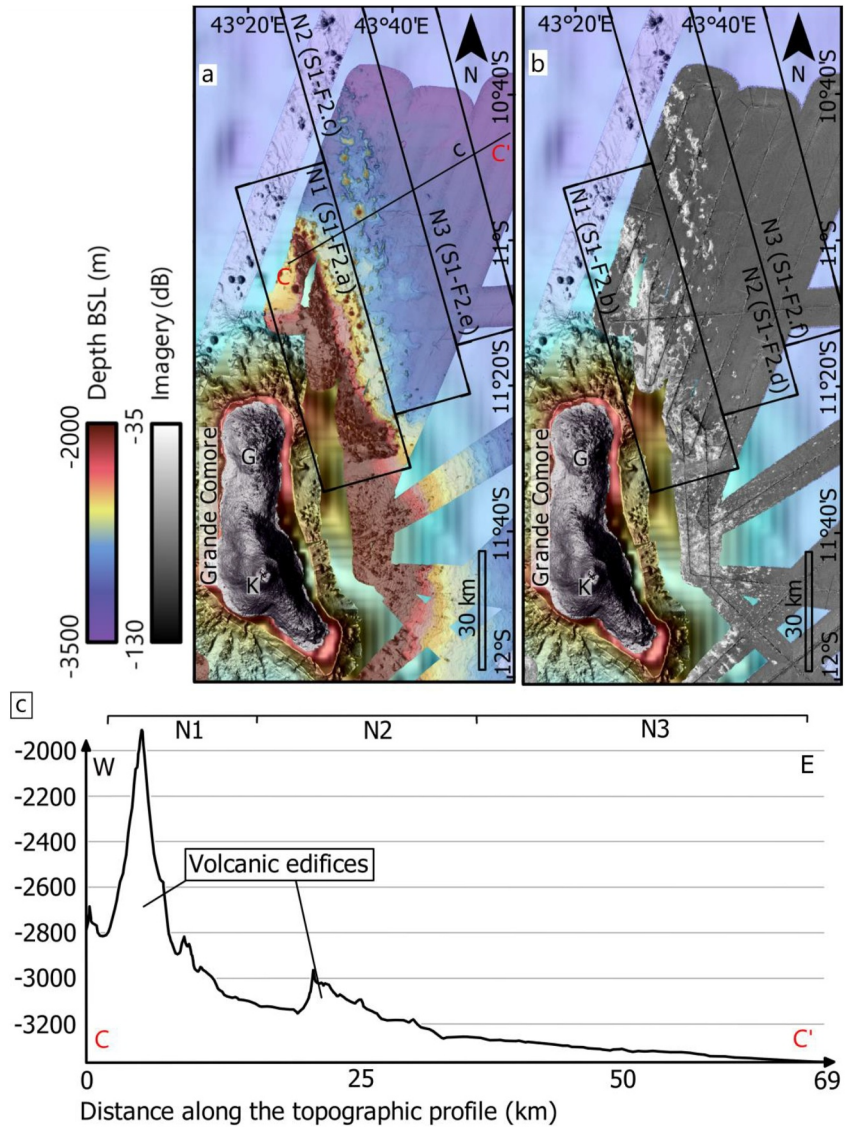

Figure 4. Bathymetric and backscatter maps in the N'Droundé area (a, b). Black rectangles: subareas identified in each of these provinces are indicated: from west to east N1, N2, N3 in N'Droundé. Red lines indicate the location of the topographic profile C-C′ presented (c). Topographic profile C-C′ (c) and main topographic features across the N'Droundé province. The extend of N1, N2, and N3 areas are indicated on the topmost part of (a).

4. Results and Interpretations

4.1. Main Characteristics of Volcanic and Tectonic Features in Bathymetry, Backscatter and Seismic Data

Most of the volcanic and tectonic structures have been identified and interpreted in the Mwezi and N'Drounde provinces using bathymetry, backscatter and seismic data by Tzevahirtzian et al. (2021) and Thinon et al. (2022). In the following section, we present them briefly. Tens of seamounts of various shapes (cones, flat dome, irregular or crescent shape edifices, elongated ridge, star-shaped volcanoes) up to 3 km-wide, 5 km-long, 800 m-high are observed on the seafloor (Figures 5a, 5b, 5c, and 5e). Some are highly reflective in the backscatter. Seamounts can coalesce to form several kilometers-wide complex volcanic features that are sometimes aligned in a NW-SE direction (Figure 5a). Numerous forced folds (folds associated with the bending and uplift of the sedimentary pile appearing as dome shaped structures (Priyadarshi et al., 2022)) are observed in the region (with a higher occurrence at Mwezi). These are large, flattened, circular or oval domes with a maximum height of 30 m and an average width of 5–6 km (Figures 5d and 5f). They display low reflectivity in the backscatter. Some of them

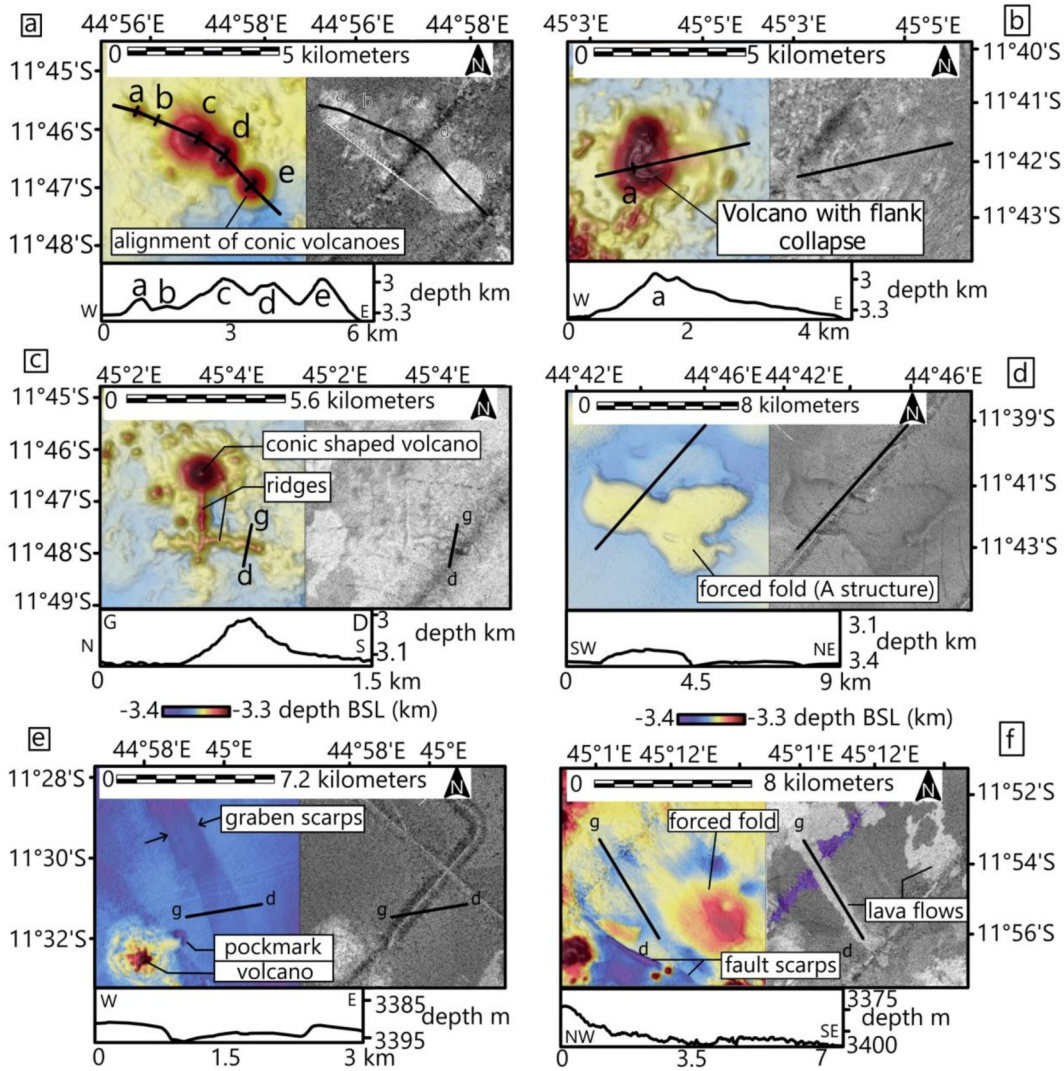

Figure 5. Bathymetry (left panels) and backscatter (right panels) of the main volcano-tectonic features identified in the Mwezi and N'Droundé volcanic provinces. Topographic cross-sections in the bottom panels with locations of the profiles on bathymetric and backscatter maps above (a) an alignment of conic-shaped seamounts. (b) A crescent-shaped breached seamount, possibly with evidence of volcanic flank collapse. (c) A cone-shaped seamount coalescent with two perpendicular ridges. (d) A forced fold (part of the "A" structure identified Figure 3a). (e) A 4 m-wide narrow graben and a star-shaped volcanic edifice. (f) Highly reflective lava-flows (facies B2 to B4, Table S2-1 in Supporting Information S1), a forced-fold and a fault scarp that are visible only in the bathymetry.

coalesce to form wider structures (e.g., structure "A," 35 km long, 60 m high, oriented N°130′E, purple ellipse in Figures 3a and 5d). Deci-kilometric lava-flows have been emplaced in the Mwezi province (Thinon et al., 2022). They are flat and indistinguishable in our bathymetry, the vertical resolution of which is too low. However, they are very clear in the backscatter data due to their high reflectivity, which is typical of fresh lava flows on the seabed (Gonidec et al., 2003; Wright et al., 1996).

In both provinces, sharp scarps have been identified and interpreted as fault scarps (Thinon et al. (2022). In the Mwezi provinces, they are oriented N130°E or NS and are up to 40 km-long and 15 m- high (Figures 5e and 5f). Some faults form grabens, 12–15 m wide. In N'Droundé province, the scarps are less numerous, smaller (up to 5 km-long, 5 m-high), and oriented N160°E.

These volcanic and tectonic structures disrupt or affect the up to 2 s. TWTT-thick sedimentary cover and are identifiable in the seismic profiles (Figures 6–8, Supplements 3 and 4, seismic facies in Table S5-1 in Supporting

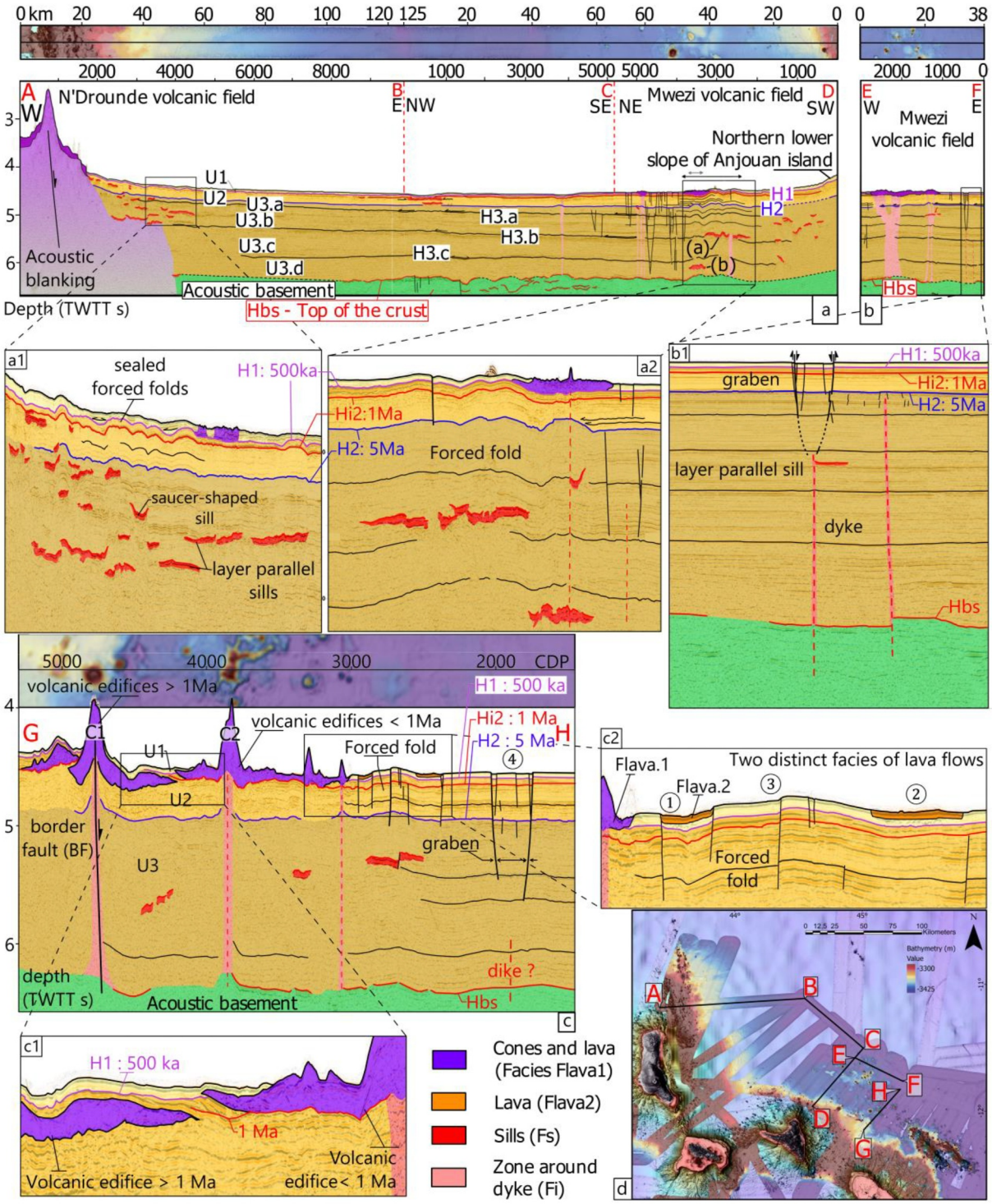

Figure 6. Interpretation of the SISMAORE 48-channel seismic reflection profiles. (a and b) Regional composite seismic profile (with a bathymetric band above) ((a) AB (MAOR070), BC (MAOR075), CD (MAOR053), and (b) EF (MAOR077) across N'Droundé, the northern Comoros abyssal plain and Mwezi and zooms (a1), (a2), (b1) below. In Beige: the thin layered seismic (sedimentary) unit U1 (facies F1 Table S5-1 in Supporting Information S1, average thickness of 33 ms. TWTT; ~28 m in using an arbitrary velocity of 1,700 m.s^{-1}). In yellow: Seismic unit U2 (average thickness: 200 ms. TWTT thick −170 m thick using an arbitrary velocity of 1,700 m.s^{-1}) with seismic facies characteristic of layered sediments (F2a and F2b in Table S5-1 in Supporting Information S1). The base of the unit U2 is a high-amplitude reflector (5 Ma old H2). In brown: the lower seismic unit U3 (on average 1.66 s. TWTT; ~2 km in using an arbitrary velocity of 2,500 m.s^{-1}) with layered seismic facies characteristics of sediments (F3a and F3b, in Table S5-1 in Supporting Information S1). The U3 unit rests on the top of the acoustic basement in green (Hbs reflector, attributed to the oceanic crust by Masquelet et al. (2023)). Purple, red and blue lines: main seismic horizon H1 (200 ka), Hi2 (1 Ma), H2, (5 Ma). Sub-horizontal thin black lines: internal

Information S1). The sedimentary cover is made of three main seismic units (U1, U2, U3), separated by two main horizons: H1 and H2, 500 ka and 5 Ma old respectively (see details on age estimation in Figure 8 and Supplement 6 in Supporting Information S1). A major 1Ma-old reflector (Hi2), internal to the seismic unit U2, is also present throughout the area (Hi2 Figures 6–8). The sedimentary cover is intruded by saucer-shaped, inclined or stratified sills ("S-events," Acocella, 2021; Infante_Peiz & Marfurt, 2017; Magee et al., 2013; Medialdea et al., 2017; Preine, Hübscher, et al., 2022; Preine, Karstens, et al., 2022; Thomson & Hutton, 2004). As observed elsewhere in the world (Shoulders & Cartwright, 2004; Stearns, 1978; Trude et al., 2003), the dome-shaped forced folds are linked to these intrusive sills. During their emplacement, the sills uplifted and faulted the sedimentary cover forming anticlines up to 5 km wide, and 20 m high (Figures 6a2, 6c2, and 7b, Figure S3-13 in Supporting Information S1). Lava flows are located within or above a thin sedimentary cover. The conic-shaped edifices and ridges are characterized by a sharp topography. Their bodies are low-reflective and heterogeneous, whereas their summit is a rough, high amplitude reflector (Figures 6 and 7, Figure S3-23 in Supporting Information S1). They may coalesce and/or stack up to form a large zone with a complex seismic signature with both strongly and weakly reflective zones (high amplitude at summit and low amplitude for the magmatic pipes, Figures 6 and 7, Figure S3-22 in Supporting Information S1). These complex internal seismic architectures have been interpreted as stacked volcanic events emplaced during several episodes (Masquelet et al., 2022). Dykes (or Non-Offsetting Discontinuity NOD in seismic interpretations, Bosworth et al., 2015; Kirton & Donato, 1985; Magee & Jackson, 2020; Wall et al., 2010) intrude the sedimentary cover (Figure 6b; Figure S3-24 in Supporting Information S1). Some lie below the narrow graben observed in the bathymetry (on Figure 6b, the antithetic normal faults system roots on the dyke at 5.25 s. TWTT depth, ∼560 m below seafloor using a velocity of 2,000 m.s^{-1}). The normal faults have a high apparent dip angle (60–80° using a velocity of 1,500 m.s^{-1}). They offset the internal reflectors of the sedimentary units by 7 ms and 20 ms TWTT (i.e., 6–20 m using a velocity of 1,700 m.s^{-1}).

This geometry has been observed elsewhere in the world by Bosworth et al. (2015) and Magee and Jackson (2020) who argued that narrow linear grabens can form above the dikes as they penetrate and propagate in the sediment.

The volcano-tectonic structures interact with each-others. The sills can be linked together by dykes (Figures 6a2 and 6b1) which take root either at the tips of the sills or at their roofs (see Figure 7a2). The magma is transported by dikes from a sill to another one into the sedimentary cover until it reaches the surface, creating volcanic edifices of various shapes and lava-flows sometimes directly above sills (Figures 6a2 and 7b). The faults guide the emplacement of the volcanic products are those are mainly observed along normal faults (Figure 6b, with a striking example Figure S4-4 in Supporting Information S1).

reflectors of the seismic U3; sub-vertical black lines: faults; dashed black line: inferred faults. Red patches: sills characterized by high-amplitude seismic reflectors (thickness of at most 50 ms. TWTT, ∼50 m in using a velocity of 2,000 m.s^{-1}). Note that the sills act as a seismic screen, attenuating or disturbing the seismic facies of the underlying units (Facies Fi, Table S5-1 in Supporting Information S1). Dark purple and thin orange patches: lava flow, volcanic cones and ridges. The cones and ridges have sharp topography, a summit underlined by a rough high amplitude reflector (sea also Figure S2-23 in Supporting Information S1) and a low-reflective and heterogeneous seismic facies (Fi, Table S5-1 in Supporting Information S1). Two types of lava are identified: one in purple (average thickness of 30 ms. TWTT; 125-m in using the velocity of 4,000 m.s^{-1} from Masquelet et al. (2022)) is characterized by a rough high-amplitude top, a continuous high-amplitude and low-frequency base and a chaotic low-amplitude internal seismic facies (facies Flava.1, Table S5-1 in Supporting Information S1). The second type in orange is the flat, characterized by high amplitude and low frequency reflectors (facies Flava.2 Table S5-1 in Supporting Information S1). Vertical pink patches (with dashed vertical red lines in zooms): vertical perturbations of the seismic units with interruption of the signal, wedges of reflectors and/or an anomalously low seismic amplitude (Fs facies, Table S5-1 in Supporting Information S1): dykes (Magee & Jackson, 2020), magma conduits (Infante-Paez & Marfurt, 2017) or seal bypass system (e.g., Masquelet et al., 2022). Pink polygons: areas where the seismic facies of the seismic unit beneath the main volcanic edifices and ridges are disturbed (either because volcanic products act as a seismic screen - acoustic blanking- or the propagation velocities are very heterogeneous and induce pull-up artifact). (a1) Saucer-shaped and layered parallel sills into the sedimentary cover, and forced folds sealed by the seismic unit U1 in the N'Droundé province. (a2) sills at various depths associated with several generations of forced folds in the Mwezi province. Some forced folds, also visible in the bathymetry, are very recent (the seafloor in folded and uplifted along with the main most recent sedimentary units). Some are older, sealed by sediment layers of U2 unit, which reflectors onlap U3, H2 being locally an angular unconformity. Note that at this place a dyke roots on a sill and reaches the surface beneath lava-flow and cone (purple). (b1) A symmetric graben (bounded by an antithetic fault system) with an intrusive dyke and a sill below. (c) interpreted GH (MAOR002) seismic section and zooms (c1), (c2) perpendicular to the Mwezi depression and across the boundary fault (BF) with forced fold, symmetric graben reaching the seafloor (with faults scarps visible in the bathymetry), dikes and sills seating deeper within the sedimentary cover, lava flows (with facies Flava.2). The scarp of the BF fault is steep (70°), 200 m-high scarp (Figure 4a), N130°E striking and segmented. Across the scarp, the seafloor, the unit U1 and base of the volcanic seamounts are offset by up to 300 m. C1 and C2 volcanic edifices along the border fault; C1 sealed by Hi2 (red) is older than C2 (emplaced above (Hi2, red).

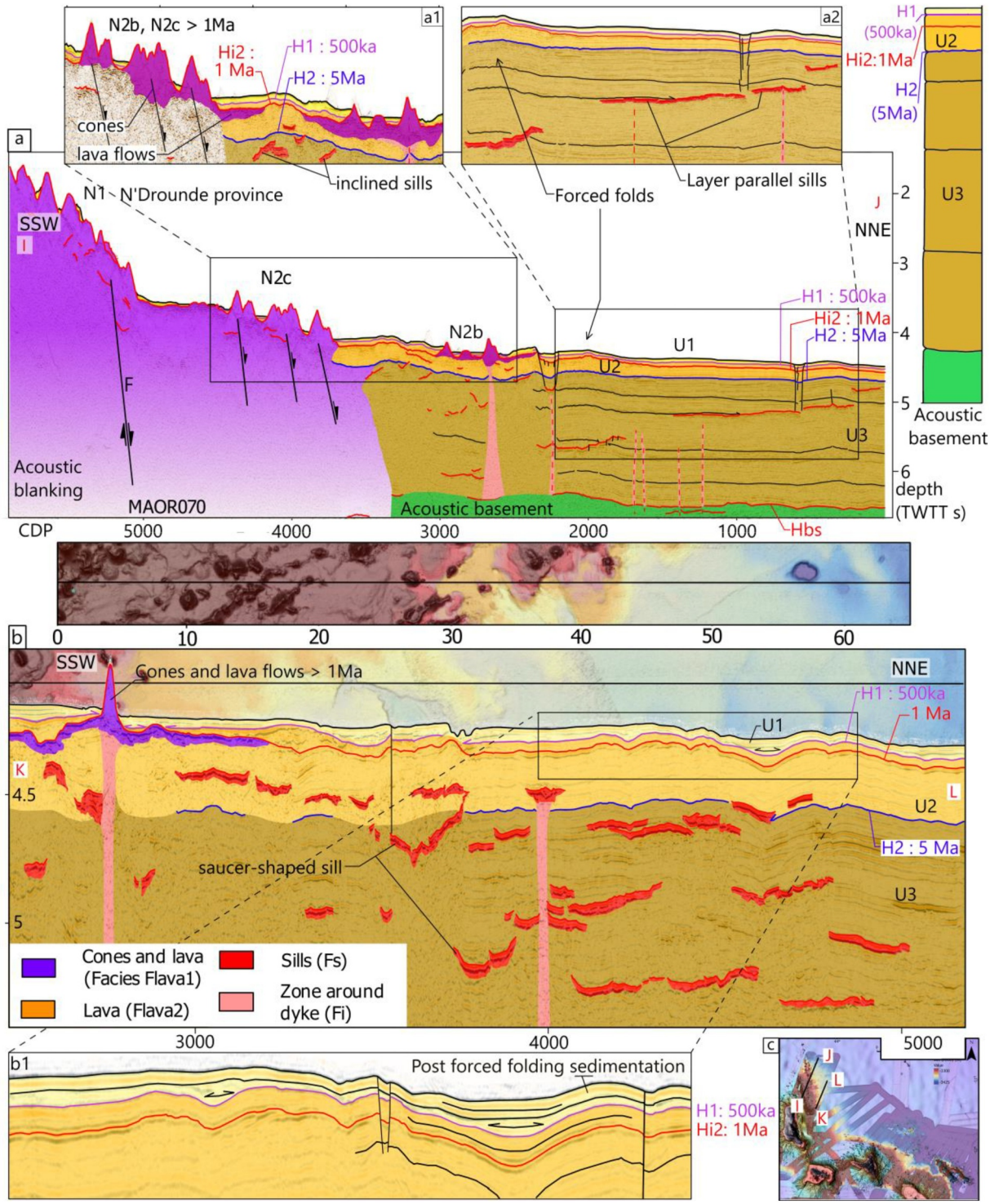

Figure 7. Interpretation of the SISMAORE 48-channel seismic reflection profiles in the N'Droundé province, symbols and colors as shown in Figure 6. (a) IJ, MAOR070 seismic section across the major NNW-SSE topographic ridges N1, N2b, and N2c with numerous volcanic cones at the seafloor and a low reflectivity seismic facies beneath (acoustic blanking). Normal faults (F being the major one) offset the seafloor, separating N1 and the N2c ridges. Beneath the N2b ridge, the seismic reflectors are disrupted by a dyke intrusion. At the NNE end of the seismic profiles, a symmetric graben with its antithetic faults, forced folds and a large set of sills at various depths are observed. (a1) Close-up view of the seismic profile on ridges N2c and N2b that shows that the volcanic cones composing the ridges are partly covered by the seismic unit U1 and the H(X?) 1 Ma old horizon. (a2) Close-up view of the seismic profile showing a staircase of sills. (b) Interpretation of the seismic profile CD (MAOR066) across the southern end of N1 ridge and the abyssal plain. The volcanic cones and the lava flows composing the ridge are sealed by the Hi2 (red)

4.2. Kinematics and Evolution of Volcano-Tectonic Systems in Mwezi Area

4.2.1. Nature and Geometry of the Structure

Detailed analysis of the morphology, orientation and organization of the volcanic and tectonic features of the Mwezi province has enabled us to distinguish three sub-zones (M1, M2, M3, along the average NW-SE trend of the volcanic province (Figures 3 and 9 with zooms in supplementary material 1 and 2 in Supporting Information S1).

Subarea M1 is the Southeastern part of the Mwezi province. It is made up of scattered and isolated seamounts and is crossed by around 5 up to 15 km-long N130°E-trending narrow grabens. The seamounts and faults are located in a depression 50 km wide and around 50 m deep (Mwezi depression, Figures 3c and 3d, which is bounded to the south by the steep (70°), 200 m-high, NW-SE-trending escarpments of a major normal fault (the Border Fault, BF).

50–100 m high seamounts have formed along the fault. Magma conduits or sets of dykes were set up along the fault planes, which likely guided the ascending volcanic products. At some places, beneath the edifices, the seismic reflectors are curved along the conduits (Figure S3-9 in Supporting Information S1). The sediments were likely dragged along and deformed as the magma rose along the fault plane (Davies & Stewart, 2005). Pull-up effect (artifact induced by high velocities) cannot be excluded, however. Volcanic intrusions along fault planes have been described in other volcano tectonic settings (e.g., Kolumbo chain in Greece, Preine, Hübscher, et al., 2022; Preine, Karstens, et al., 2022; Taranaki Basin in New Zealand, Giba et al., 2013).

M2 subarea, in the center part of the Mwezi province, has the highest concentration of seamounts and lava flows. The lava patches overlap and become increasingly reflective toward the north- west (Figure 3a, Figure S2-1 in Supporting Information S1). This change in intensity (see facies Table S2-1, and S2-2 in Supporting Information S1) may suggest that the lava flows get younger toward the Northeast (Figure 10) as older lava flows are less reflective when covered by a very thin sediment layer (Mitchell, 1993). However, we cannot rule out the influence of topography or nature of the lava. The numerous grabens observed in M1 extend into this sub-area. They may cut through cones or lava flows, which implies that they post-date the emplacement of volcanic products on the seafloor. Several volcanic cones are aligned with fault scarps, suggesting that the faults controlled the emplacement of the volcanic products. For example, the shape of the L1 lava flow indicates that it flowed into a graben (Figures 5f and 10; Figure S2-1 in Supporting Information S1). In places, volcanic products cover the fault scarps and post -date them.

In M3 subarea, a large structure named "A" is a N110°E alignment of coalescent flat top domes (Figures 3a and 9a). We also observed an impressive set of very narrow linear grabens (1.5 km wide), 5 m deep and up to ∼9 km long, arranged radially (orientations from N110°E to N45°E) and departing from the central subarea M2 (Figure 9a). Below a graben, we observe a dyke (Figure 6b1). Although we were not able to image all the grabens with seismic data, it is likely that these grabens are all coupled with a dyke which is rooted at the base of the antithetic bounding fault (BF) system (in the center of the graben). These grabens formed during the propagation of dykes.

4.2.2. Chronology of the Magmatic and Volcanic Processes

The architecture and stratigraphy of the volcanic structures in the Mwezi area indicate several phases of magmatic and volcanic activity (Figures 6 and 8, Figures S3-9, S3-10, S4-3, S4-4, and S4-9 in Supporting Information S1). The lava flows observed in the Mwezi depression in the central M2 subarea were emplaced above the 500 ka-old seismic horizon H1, suggesting that they are younger than 500 ka (Figure 6). This is in agreement with the ∼200 ka age of a basaltic lava sample dredged in this area (Rusquet et al., 2025). Three generations of forced folds have been identified. The youngest generation folds the seafloor and is visible in the bathymetry because the post-deformation sedimentary cover is thin or non-existent ("A" structure in zone M3, seismic profile CD, Figure 6a2,

reflector and are thus older than 1 Ma. An impressive set of saucer-shaped, layer parallel and inclined sills associated to forced folds is also observed. (b1) Close-up view set of the deformed uppermost sedimentary layers above the set of saucer-shaped showing a generation of forced folds (and thus sill intrusions). The forced folds are sealed by the U1 unit in the onlap. The H1 seismic reflector, base of the unit U1 and top of the forced fold, is uplifted and folded itself. In this case, it is locally an angular unconformity. Meaning the deformation, and thus the sill intrusions occurred at or prior to 500 ka.

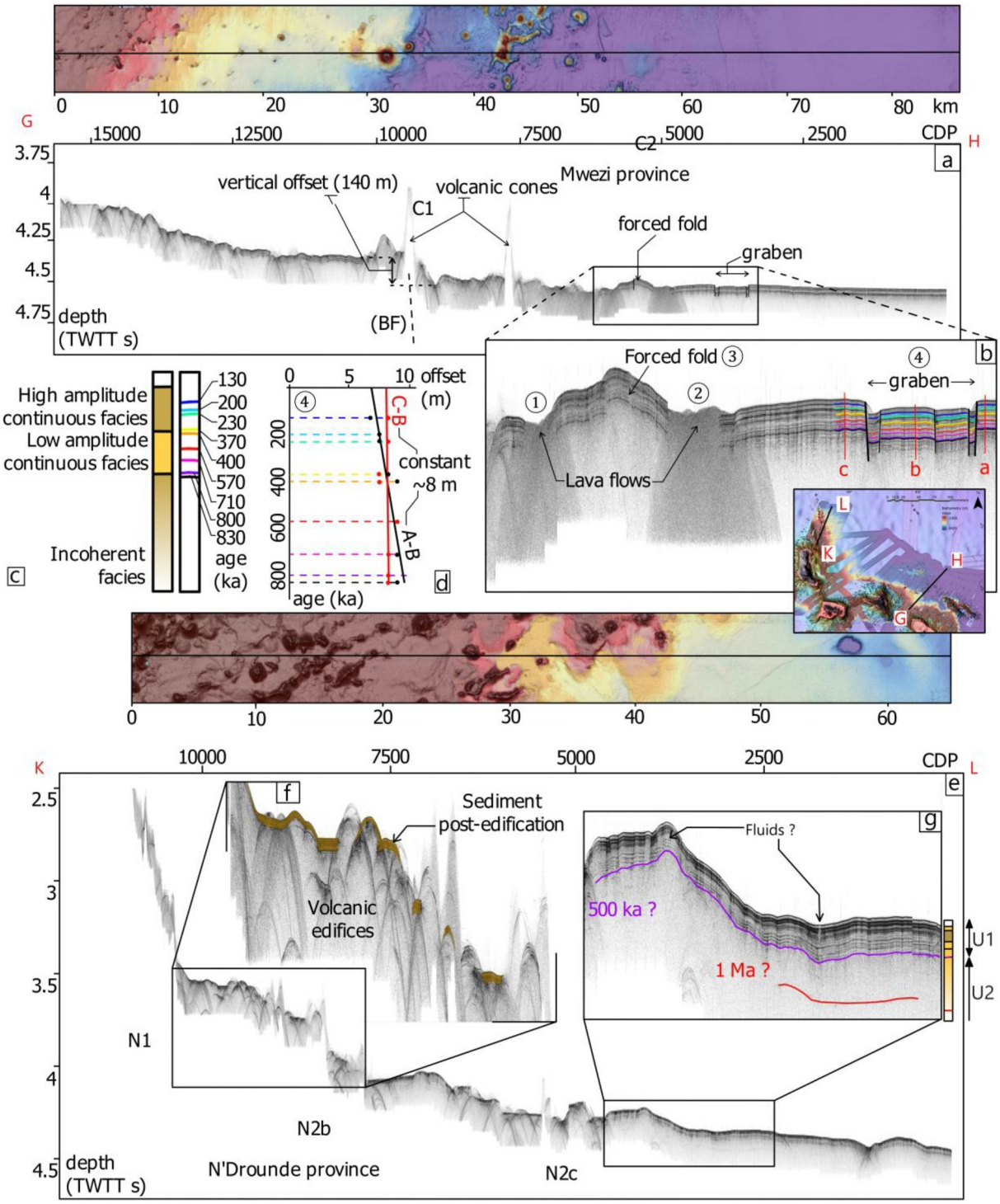

Figure 8. (a) Interpretation of the Sub-Bottom Profiles (SBP, AB, profile MAORSDS002) in the Mwezi province across the volcanic cones C1 and C2, the border fault BF, a forced fold and a narrow symmetric graben. (b) Close-up view of the forced folds (numbered 3), the lava flows (numbered 1 and 2) and the graben (numbered 4). The main seismic horizons colored across the graben were correlated with the main sedimentary units identified in the core MD21-3602 (c). Red bars in (b) indicate the place along the profile where the in-depth position of each colored horizon is compared across the faults to estimate their offset by faulting through time. (c) A core-like sample in the SBP with the main seismic facies in beige colors compared to the main sedimentary units with ages (colors as for the main seismic horizons in (b). (d) Black and red points (with lines as an interpolation) are the offsets of each colored seismic horizons across the bounding faults of the graben numbered 4 between sections A and B and B and C, respectively (red line on b). All seismic horizons are offset by the same amount (about 8 m, estimated by using a seismic velocity of 2,000 ms^{-1}) implying that faulting postdates the sedimentation and is very recent. (e) Interpretation of the SBP profile CD (MAORSDS0070) in the N'Drounde province across the N1, N2b, and N2c volcanic ridges. (f) Close-up view of profile showing that the volcanic cones of N1, N2b, and N2c are covered by the sediment pile

Figure S4-9 in Supporting Information S1). The forced folds of the second-generation are covered by a thin post-200ka sedimentary layer (Figure S4-9 in Supporting Information S1). The oldest third generation is covered by the seismic unit U2, which internal reflectors onlap the 5 Ma-old H2 horizon when folded (Figure 6a2). This indicates at least three magmatic events (5 Ma, older than 200 ka and younger than 200 ka). This is a minimum number, however, because (a) our observations depend on our data network and its resolution, so it is possible that we have missed some generation of forced folds; (b) A forced fold can be cumulative, resulting from stacks of sills from different generations (Magee et al., 2013); (c) Sills can intrude the sediments without deforming them (Magee et al., 2013).

The Sills are concentrated mainly in the U2 and U3 seismic units at four main depths: around 5.25 s. TWTT, 5.5 s. TWTT and 6 s. TWTT and 6.3 s. TWTT (i.e., ∼6.6, 6.9, 7.5, and 7.9 km-depth BSL using a velocity of 2,500 m. s^{-1}, Figure 11).

At least two generations of volcanic edifices are observed in the M1 subarea: C1 along the BF and C2 in the Mwezi depression. C1 lies below the Horizon Hi2 (red) whereas C2 lies above, implying that C1 emplaced before 1 Ma and C2 after 1 Ma (Figure 6c, Figure S3-9 in Supporting Information S1).

Both cones are covered by the seismic unit U1, suggesting that the eruptions occurred before 500 ka.

The graben observed in the M1 subarea are very recent and their BFs offset the most recent sedimentary layers and the seafloor by the same amount (∼8 m, Figure 8a). Although it was not possible to observe the associated dikes below the graben in subarea M1 because they are likely deeper than in the M3 subarea (the grabens being wider), we inferred that these grabens were also formed by dyke intrusion.

4.2.3. Estimation of Dikes Opening Values and Lava Flow Volumes

Given the dip of the graben BF in M1 subarea (60–80°), an offset of 8 m along them would mean that the dike below has opened by 8 ± 5 m. We identified four main grabens in the Mwezi depression in the M1 subarea. Their BFs offset the most recent sediments by 8–10 m. We estimate grossly a total opening of ∼32 ± 20 m of the system of dikes.

We calculated the volume of lava at the surface (32 km^3) by multiplying the total surface area of the lava flows estimated from the backscatter map (708 km^2) by the average thickness of a lava flow estimated from seismic data (45 m using seismic velocities of 2,000 $m.s^{-1}$). By multiplying the average thickness of a sill of the Mwezi volcanic field (65 m thick using velocity of 2,000 m/s) by the total forced folded surface in bathymetry (493 km^2, by making the assumption of the surface of a forced-fold being an indicator of that of the sill below), we estimate the volume of magma in sills (32 km^3—volumes intruded in the lithosphere, under the sedimentary cover are not accounted). The ratio between intruded and extruded volumes is 1:1. This is a rough estimation however as the volumes of the dykes are not included (we have no information on their depth extension). The ratio may be lower.

4.3. Kinematic and Evolution of Volcano-Tectonic Systems in N'Drounde Area

Three main subareas (N1, N2, N3 Figure 4a, Figure S1-2 in Supporting Information S1) are defined in the N'Droundé province from the distribution and arrangement of volcano-tectonic structures.

N1 is a morphological ridge, 70 km long and 13 km wide, oriented NNW-SSE, Located between 3,400 and 850 m BSL along the northwestern insular slope of the Grande Comore Island. It is made up of many coalescent conical, round, or elongated volcanic seamounts. In its southern part, closest to the Grande Comoros insular shelf, the ridge bends clockwise to reach N130°E. Small depressions can be seen at the top of the westernmost major topographic ridge N1 (Figure 9b). These are probably successive rift zones parallel to the main axis of the ridge.

N2 is a morphological ridge 60 km-long and 15 km wide oriented NNW-SSE. It is subdivided into three sub-features (N2a, N2b, N2c). N2a and N2b are two 30-km-long alignments oriented N175°E of conical edifices

of the U1 unit (in yellow) implying that this unit postdates the edification of the ridges. (g) Close-up view of the SBP profile in which we show the position of the main 48 channel seismic horizons (H1 at the base of U1 and the 1 Ma Hi2 (red)) as estimated by comparing the SBP and 48 channel seismic acquired at the same position. H1 (500 ka) is well identified at the base of a sedimentary unit characterized by high amplitude horizontal parallel reflectors are observed (high and low amplitude continuous facies).

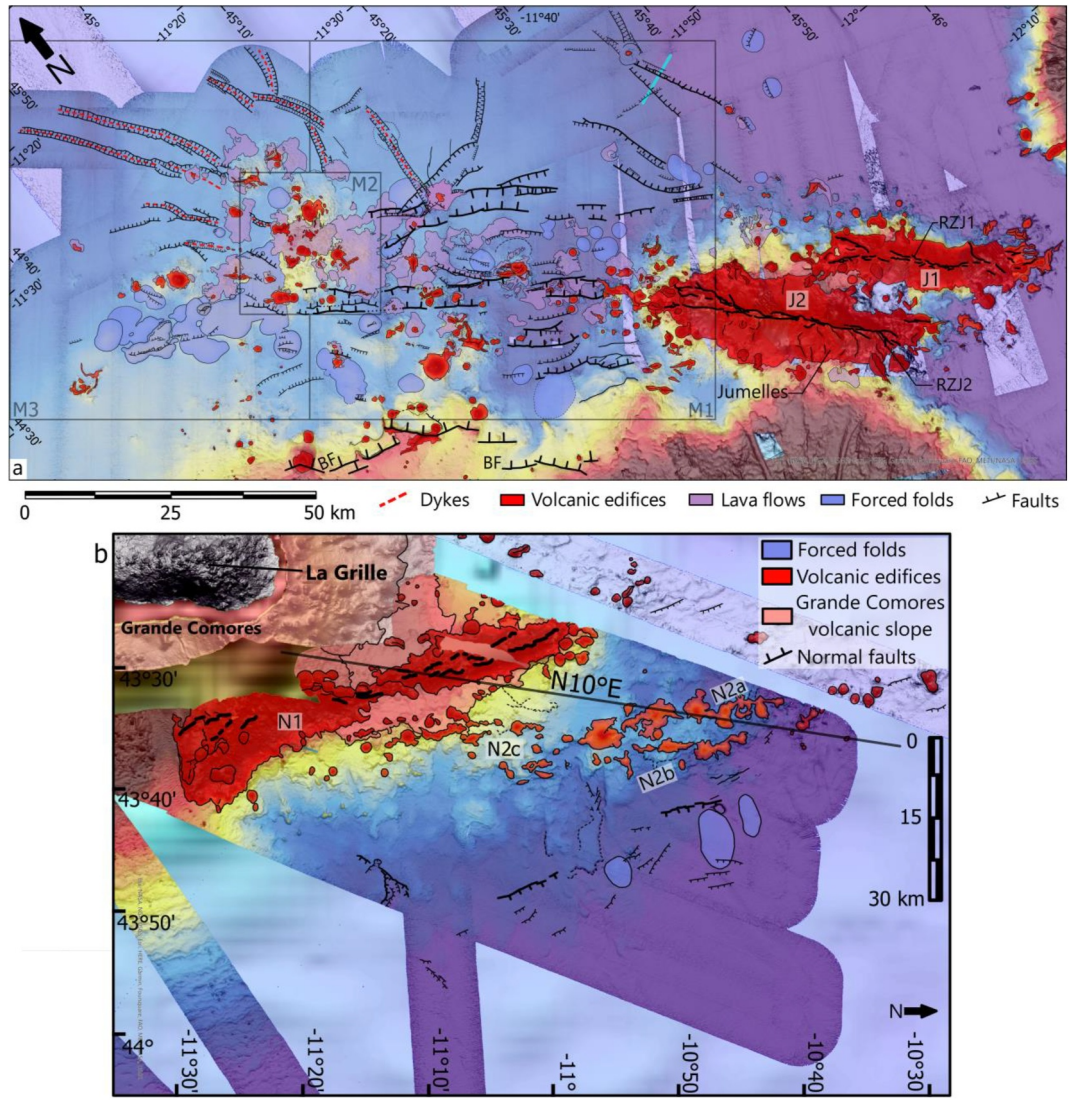

Figure 9. The rift systems of Mwezi-Jumelles (a) and N'Droundé (b). Black lines with ticks: normal faults; thick black lines: rift zones; Light pink polygons: volcanic products (lavas-flows and seamounts). Light blue polygons: forced folds. Red dotted lines: dykes identified in seismic sections whose inferred traces are projected to the surface at the center of long and narrow grabens.

and ridges up to 400 m-high. N2c is a 20 km-long N10°E striking alignment of smaller (up to 200 m-high) edifices and ridges.

A thin, weakly reflective sedimentary layer (75 ms. TWTT-thick) estimated at 1 Ma covers the volcanic structures of the morphological ridges N1, N2b, and N2c (Figure 7a1 and Figure S3-21 in Supporting Information S1). This implies that the main topographic ridges were formed before 1 Ma.

N3 is located 60 km off Grande-Comore Island to the north. It is a made up of three ellipsoidal (elongated in a E-W direction) dome shaped forced folds, 10 m-high and 10 km-long, and of six fault scarps 2 km-long and 1m-high, N170°E, running parallel to the ridges N1 and N2. The forced folds are sealed by the seismic unit U1, which is in onlap on the H1 unconformity with sometimes thin wedges. This implies that the end of deformation is post- to syn-H1 at around 500 Ka. We have observed numerous sill intrusions of various shapes, lengths (up to 4 km long) and depths beneath the forced folds. An impressive stack of saucer shape forming a staircase geometry lies in the western part of the seismic profile (Figure 7a2).

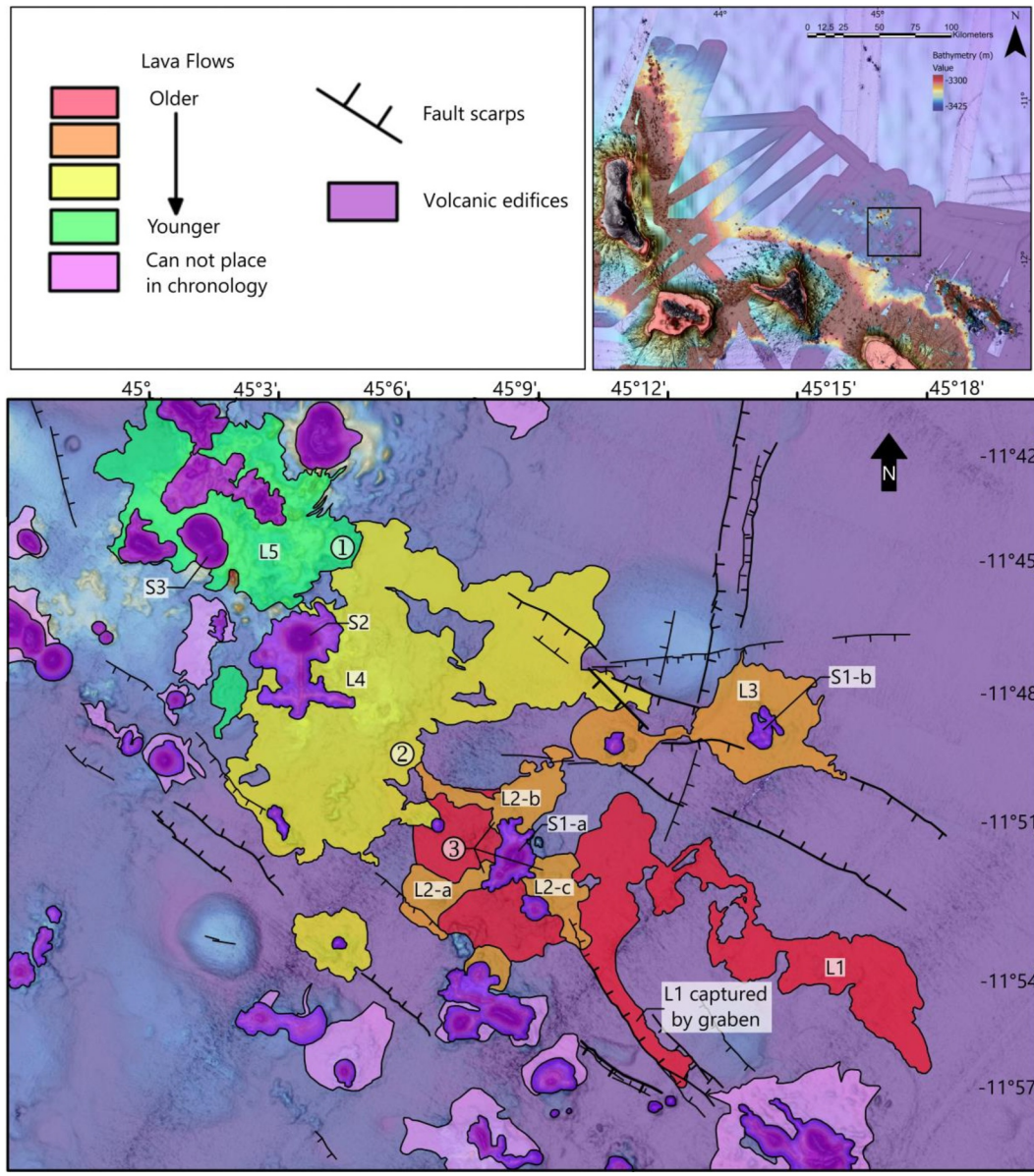

Figure 10. Relative chronology of a series of lava flows in the subareas M1 and M2 of the Mwezi volcanic province based on their backscatter facies and disposition. Red to green colors: younger to older lava flows L: L5 overlaps L4, L4 overlaps L2-b, L2-a, L2-b, and L2-c overlap L1. Light purple: scattered lava flows L (outside the series). Dark purple patches: seamounts S from which the lava flows may originate: L1, L2a, L2b, L2c from S1a, L3 from S1b, L4 from S2 and L5 from S3. The lava series and the seamount emplaced along the N130°E graben and are aligned with them. The graben bounding faults either cut across the lava flows (implying that they postdate them) or guide their emplacement (implying that they predate them).

The ridges of the N'Droundé province arrange in right stepping échelons, which form a descending staircase along the eastern insular slope of Grande-Comore Island. They likely set up along normal faults where scarps offset the seafloor by a minimum value of up to 350 m (Figure 7a, Figure S3-23 in Supporting Information S1).

In this area, most of the volcanic and tectonic structures are sealed by the most recent U1 unit and are not visible (or smooth) in the bathymetry. The lava flows lie in the seismic unit U2 (Figure 7a), implying that the most recent volcanic products are older than those in the Mwezi area, older than 500 ka.

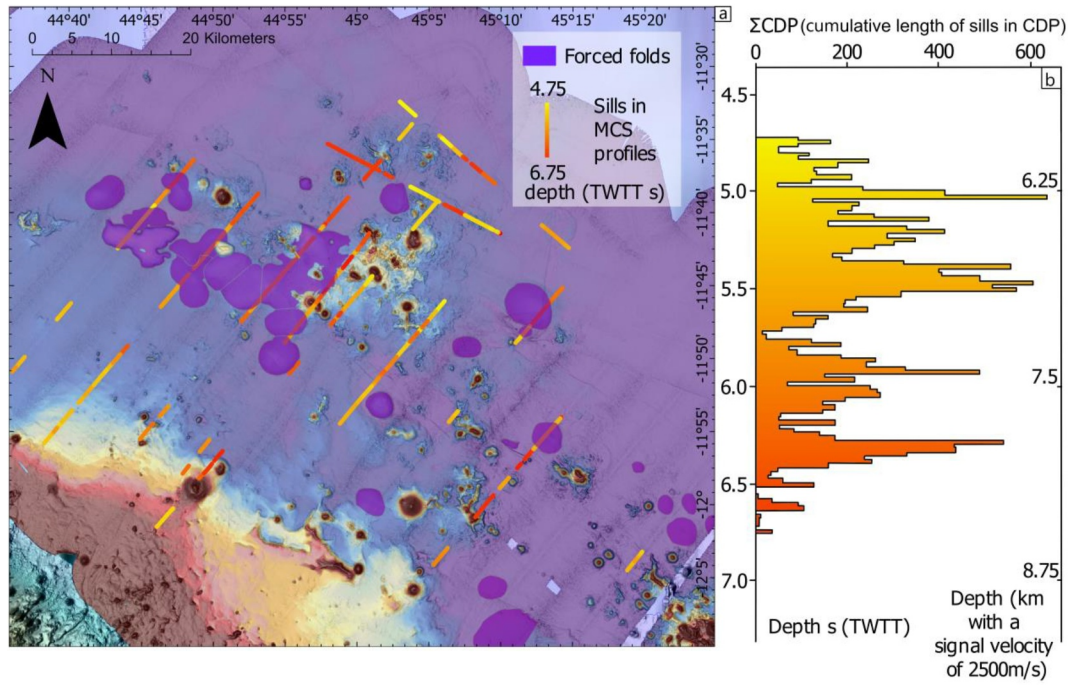

Figure 11. Spatial (a) and depth (b) distribution of the sills in the sedimentary cover of the Mwezi province identified from the 48-channel seismic profiles. (a) Purple patches: extent of forced folds at the surface. Reddish to yellowish lines: depths (in s. Two-Way Travel Time, TWTT) of the sills observed along the seismic profiles. (b) Histogram showing the cumulative length of sills (units are expressed in common depths points CDP (the distance inter CDP is 12.5 m) as a function of depth with a value every 10 ms TWTT, between 0 and 7s (the depth in km is indicated on the left considering an average velocity of 2,500 m.s^{-1}). Sills are mainly concentrated at four depths, around 5.25, 5.5, 6 and 6.3 s. TWTT.

5. Discussion

5.1. Birth and Propagation of Mwezi and N'Droundé Rifts

In the Mwezi province, a 50 km-wide, N130°E striking asymmetric depression up to 25 m-deep (Mwezi depression) is bounded by the 70 km long Border Fault system (BF) running along the insular slopes of Mayotte and Anjouan islands. No fault is observed to bind the Mwezi depression to the North in our data set (although it could be very small or located further north of our study area).

This depression is parallel to and lies at the tip of the Jumelles volcanic chains at the top of which narrow rift zones (2 km-wide depressions) have been identified (RZJ1 and RZJ2, Figure 9a). The Mwezi depression is an asymmetric graben into which other narrower (4 km wide) symmetric N130°E-striking grabens lie in the extension of the Jumelles rift zones RZJ1 and RZJ2. While not observed in the seismic profiles, those grabens are likely the result of dike propagation from J1 and J2 into Mwezi. The system extends north-westwards into the M2 subarea and beyond, for more than 25 km, across the "A" group of very recent forced folds. This group, along with the radial set of narrow grabens and dikes depart from the central M2 zone. Radial sets of dikes were observed elsewhere in various volcanic zones globally; in Colorado (Muller, 1977; Odé, 1957), in the Galapagos (Chadwick & Howard, 1991), in East Antarctica (Hoek, 1995) and around the Alba Patera Martian volcano (Cailleau et al., 2003). They depart from the center of volcanic edifices, whose load disturbs the regional stress radially, controlling the distribution of the dyke swarm (Acocella & Neri, 2009; Paquet et al., 2007; Srivastava et al., 2019). It is worth nothing that our radial dyke swarm lies on a flat seafloor (around 3,400 m deep BSL). Odé (1957) showed that the propagation of dykes in the sedimentary cover is directly controlled by the ambient stress field, with the dyke progressing orthogonally to the minimum compressive stress σ_3. A simple 2D numerical model (see detail in Supplement 8 in Supporting Information S1) indicates that the distribution of the dikes in the Mwezi province can be accounted for by a local stress perturbation of a N40°E regional extension. This perturbation lies in the central M2 area, where the largest concentration of volcanic edifices and lava flows has been observed. It is asymmetric, acting only on one side of the medium, in the M3 subarea. A local stress

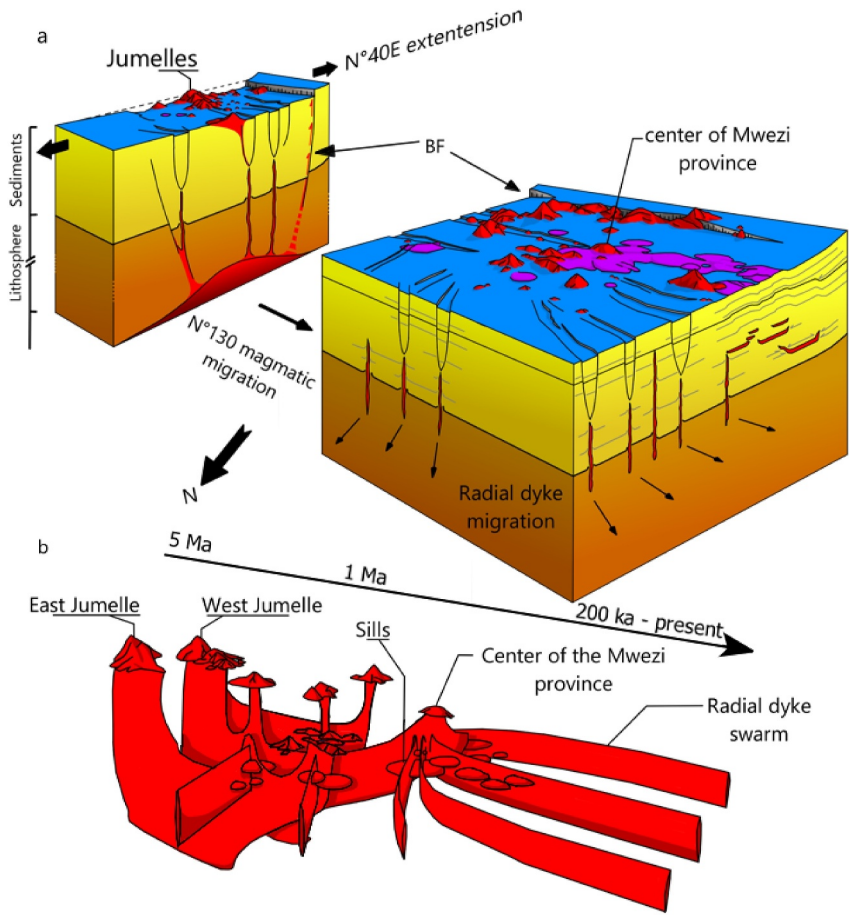

Figure 12. (a) Sketch of The Jumelles-Mwezi rift system across the Lithosphere (not at scale) with (b) showing the inferred plumbing system in 3 D. The rift is asymmetric, bounded to the south by the major BF normal fault. It accommodates a N40°E regional extension. A main magmatic reservoir (in red) is in the lithosphere beneath the Jumelles ridges and is associated with a set of parallel or oblique dikes (in red) injected from the main reservoir in the Mwezi area during rifting events. The rift propagated northwestward between the Jumelles (5 Ma) and the most recent "A" forced fold structure formed during sill injections less than 200 ka ago. The tip of the propagating rift is inferred to be in the center part of Mwezi, where a higher concentration of volcanic products is observed, and from with depart several radial dikes. In yellow: sedimentary cover, in orange: lithospheric basement.

perturbation at the tip of a propagating crack accounts for such a geometry (i.e., oblique normal faulting at the tip of a dike, Feuillet et al., 2004).

The Mwezi and Jumelles provinces are part of the same volcanic system. This system has propagated northwestwards in the Mwezi depression, as shown by decreasing ages of volcanic seamounts and forced- folds, in this direction. The system presents all the characteristics of a propagating rift (Figures 12 and 13). A radial dyke swarm developed at the propagating tips of the rift. In addition to the swarm of radial dikes, we observed several NS striking grabens oblique to the main structures of the Mwezi volcano-tectonic provinces along the strike of the rift. The later structures (numbered 1 to 4 in Figure 13) may have gradually formed at the tip of the rift as it propagated toward zone "A." Such structures could be compared to splay fault networks (horsetail or wing cracks) observed at the tip of a propagating main fault (Perrin et al., 2016).

There is no oblique dike on the other side of the rift likely because of the islands and the insular slope act as a buttress zone preventing diking in this direction. In general, splay fault networks are asymmetric (Perrin et al., 2016).

The N130°E Jumelles-Mwezi rift system began to form-5 Ma-ago when the volcanism initiated at the Jumelles chains, which are the oldest and highest structures of this rift.

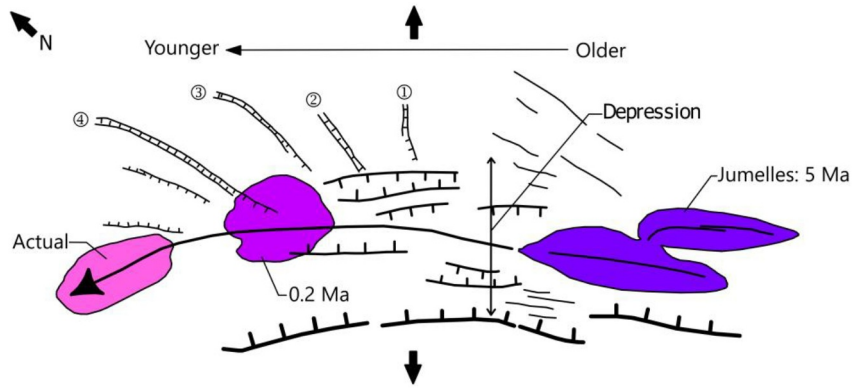

Figure 13. Evolution of the Jumelles-Mwezi rift. The rift began to form 5 Ma yr-ago with the formation of the Jumelles ridges (dark purple). It then migrated northwestwards to reach the center of the Mwezi area (purple) 200 ka ago and then in zone pink are where the most recent evidences of magmatism are seen (set of forced folds "A"). The narrow radial dykes and graben numbered 1 to 4 formed less than 200 ka ago at the tip of the rift as it propagated in zone A (pink), with the number corresponding to the order of graben formation (1, then, 2, 3 and finally 4). Faults as in Figure 9. Black arrow: regional extension (N40°E).

It then propagated northwestwards to reach the M1 subarea in the Mwezi province around 1 Ma (based on the ages of the volcanic cones over BF). The BF, which is part of the system, likely began its activity at the same period. The system then propagated again northwestward through the M2 subarea in the recent times where we identified sill intrusions younger than 0.2 Ma.

The existence of very young surfacing grabens suggests very recent dike intrusions throughout the rift (Figure 12a). Lavas were mainly set up along the BFs of the graben during the dike propagation (Figure 13).

Staircases of sill intrusions (with dykes in between sills) have been identified. This suggests that the magma propagated from deep sources (beneath the sedimentary cover) upwards via a series of sills and dikes following favorable tectonic paths. Our observations agree well with that of a single deep source feeding a laterally extensive sill complex (Magee et al., 2016) instead of the more traditional model (dikes feeding the eruption directly above multiple melt sources, e.g., review from Acocella (2021)).

The magmatic source may be located beneath the highest and older Jumelles volcanic chains (more evolved structures). During Plio-Quaternary rifting episodes, it is likely that the magma was transported from the Jumelles to reach the M2 and M3 subareas of the Mwezi volcanic province via horizontal sills and dyke systems as the rift propagated. To our knowledge, this is the first time that the surface expression of a vast network of narrow grabens associated to dykes has been documented over such distances. We showed that every system grabens and dykes is very recent (offsetting by the same amount all the recent post 1 Ma sedimentary cover and the seafloor). They thus likely formed coevally and are the remnants of the last major rifting episode.

We estimated that a total opening of at least ~32 ± 20 m was accommodated by the network of dykes in the Mwezi depression, probably during this single episode of rifting. It is thus possible that the Jumelles-Mwezi rift evolved and propagated during main volcano-tectonic pulses as observed elsewhere. Indeed, Hubsher et al., 2015; Preine, Hübscher, et al., 2022; Preine, Karstens, et al., 2022, documented five rift pulses at the Santorini rift with openings of hundreds of meters. They also showed that the rift BF moved incrementally during the rifting event in the Santorini rift (Preine, Hübscher, et al., 2022; Preine, Karstens, et al., 2022).

The main BF fault may have moved with the opening of the dyke during this rifting episode, accommodating part of this extension. We cannot document this from the seismic profile since the continuity of the reflectors is not clear across the fault because volcanic cones have been set up on the fault. The value of ~32 ± 20 m of opening is therefore a minimum value, which is still of the same order of magnitude as that estimated during the main rift pulses at Santorini rift.

Rifting events involving deep reservoirs and kilometers long dike systems have been observed elsewhere during rifting episodes in Afar (Ebinger et al., 2010; Grandin et al., 2009; Hamling et al., 2009) or in Iceland (Sigmundsson et al., 2015). Those rifting episodes contribute to accommodate regional extension across the system

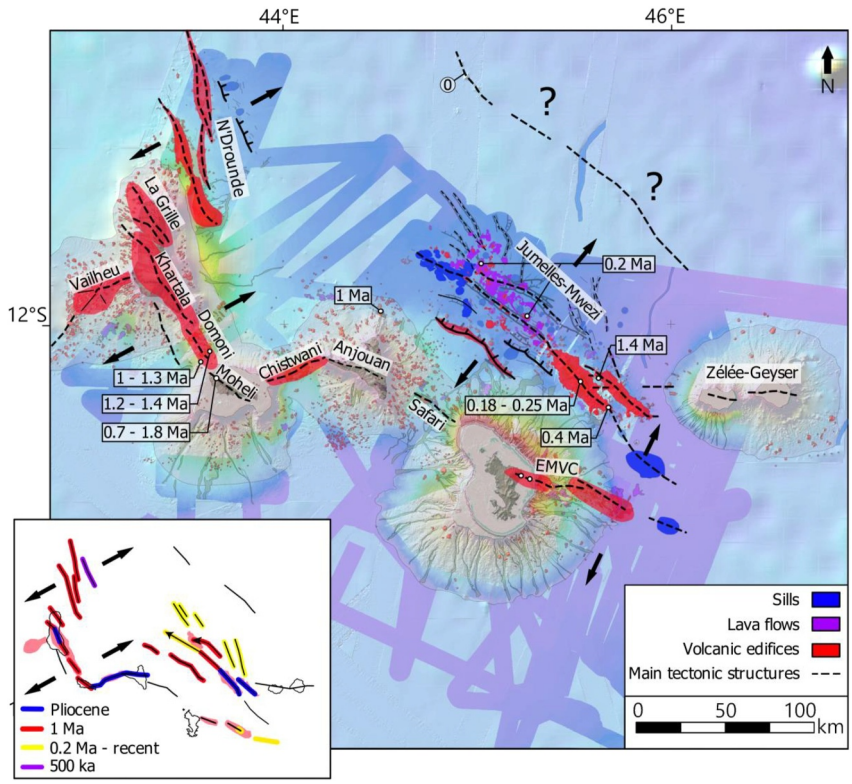

Figure 14. Distribution and evolution of the rifts in the Comoros archipelago with a simplified sketch of the structure with ages (left inset) and the larger scale geodynamic setting of the rifts (right inset, with main elements as in Figure 1 and this study). The Mwezi and N'Drounde rifts are part of a larger regional scale system composed of transtensional volcano-tectonic systems arranged *en-échelon* along the Comoros archipelago. Structures from Feuillet et al. (2021), Thinon et al. (2022) and this study. The N'Droundé N1, 2, 3, ridges, La Grille edifice, the Karthala rift zones, and Domoni ridge (Dashed black line surrounded by red elongated polygons) organize in right-stepping (sinistral) échelons in a N20°E direction to accommodate a N40°E directed extension (black thick double arrows) and are part of a same rift system. From this study and K-Ar dating (indicated in white transparent boxes of volcanic products, Rusquet et al., 2025), and from Masquelet et al. (2023), the system initiated about 2 Ma ago with the edification of the submarine part of the Grande-Comores Island and then propagated both south-eastwards and north-westwards to form the Domoni and N'Droundé ridges. The N'Droundé–Domoni rift was arranged in a left-stepping (dextral) échelon in an E-W direction with the Mwezi- Jumelles rifts and other transtensional structures (EMVC, Anjouan rift zones, Safari ridge) in the archipelago to accommodate the N40°E directed regional extension. Dashed black lines with question marks (numbered 0): a possible transtensional structure along which the seamount and faults aligned in a N130°E direction is visible in the bathymetry. As proposed previously by Famin et al. (2020), Feuillet et al. (2021), and Thinon et al. (2022), the rifts developed in an E-W dextral shear zone in which they accommodate a N40°E-striking extension. Their kinematics and evolution indicate that they are propagating rifts and as proposed earlier by Feuillet et al. (2021), we infer that they were created in a transfer zone between the offshore branch of the EARS (Kerimbas graben) and the Malagasy Rift System (Antongil bay/Alaotra graben).

and last several years. During the 2005 rifting event in Afar, the dykes opened by 8 m (Wright et al., 2006), which is a value equivalent to the 8 ± 5 m we estimated for a single dike opening in the Mwezi depression. It is possible that multiple diking events (each associated with a dyke formation) occurred during this most recent and unique event over the last 1 Ma rift-pulse in Mwezi. This rift pulse may have lasted a few years or tens of thousands of years. With only around 40 seismic reflectors identified in the 1 Ma old sedimentary sequence (25 ka on average between the deposition of two reflectors), it is not possible to distinguish a rifting event that would have lasted a few years or a few decades from our data.

In the volcanic province of N'Droundé, we have identified several sets of cones and lava flows that gather to form N160° ± 10°E striking ridges organized in sinistral echelons along the N20°E direction. The main ridges N1 and N2 likely formed before 1 Ma ago along the major fault system (Figure 14). To the North-East, in the abyssal plain, the forced folds are younger (500 ka). The main magmatic source of the sill systems could be located beneath the main major topographic ridge (N1) or the island of Grande Comore, where the volcanism is young (La

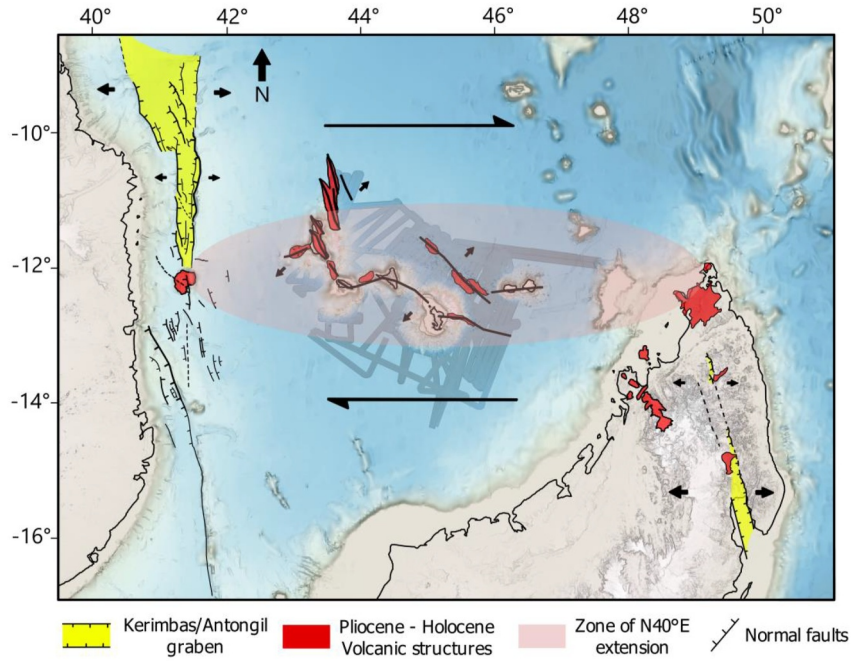

Figure 15. Volcano-tectonic structures of the Comoros archipelago within the geodynamical context of the North Mozambique Channel. The dextral shear geodynamics creates a large band where a N40°E extension dominates between the offshore Southeastern branch of the EARS (Kerimbas graben) and the Malagasy Rift System (Antongil bay graben). The N130°E–N170°E rifting systems of the Comoros archipelago (resp: Mwezi and N'Droundé provinces) form to accommodate the N40°E extensional strain.

Grille volcanic complex) and active nowadays (Karthala volcano). The onset of volcanic activity on Grande-Comore Island was estimated at 2 Ma by Masquelet et al. (2023). The N1 and N2 ridges are younger. The volcanism might have migrated toward the NNE, from Grande-Comores to the abyssal plain.

The ages we estimated for the edification of the N1 and N2 ridges also coincide with those of the Domoni volcanic chain and Moheli Island (0.7–1.8 Ma, Rusquet et al., 2023). The latter authors suggest that the Domoni volcanic chain and the currently active Karthala volcano belong to the same volcanic system. The ridges N1, N2, N3, Grande Comore Island and the Domoni volcanic chain were likely built during an important submarine magmatic event that began 2 Ma ago and continued until 500 ka-ago in the Northeastern part of N'Droundé (N3). Although submarine volcanic activity may have persisted along the N1 ridge at the summit, along rift zones or on the flanks, the submarine structures N1 and N2 likely completed their main phase of edification and propagation 1 Ma ago. This coincides strikingly with the emergence of Grande-Comores Island and the onset of aerial volcanism (between 1,200 and 800 ka from e.g., Bordenca et al., 2023; Quidelleur et al., 2022; Rusquet et al., 2023 and reference therein). Since then, the main volcanic activity may have concentrated to form the Karthala shield volcano, probably above the main reservoirs or at La Grille volcano (Bachèlery, Lenat, et al., 2016).

Petrological composition of recent lavas of the Karthala indicates multiple magma chambers, the main one lying 30 km below the Karthala volcano (Desgroslard, 1996). This might be the main source that contributed to the edification of the older submarine ridges in the area (N'Droundé ridges, Vailheu volcanic chain and the Domoni volcanic chain) and La Grille volcano through horizontal diking processes before 500 ka.

5.2. Origin of the Rifts in the Framework of the EARS

We showed that the N130°E striking volcano-tectonic structures of the Jumelles-Mwezi system are remnants of rift pulses that occurred between 5 Ma and present day to accommodate a N40°E regional extension. The Jumelles-Mwezi rift is the largest in the whole archipelago (150 km long and 60 km wide in total, Figure 14). About 100 km, northeast of the Mwezi-Jumelles system, there is a N130°E-striking alignment of cones and fault scarps that are parallel to the Mwezi volcano-tectonic field (numbered "O" in Figure 14). Southwards, the eastern

part of the East Mayotte Volcanic Ridge (EMVC) is also oriented N130°E on average (Feuillet et al., 2021) and belongs to the Mayotte volcanic system (from Masquelet et al. (2023)). It is parallel to the main structures of the Mwezi volcano-tectonic province. In between Mayotte and Anjouan, the safari ridge is also oriented N130°E.

All these ridges may result from interactions between tectonic and volcanic processes to accommodate a regional N40°E extension (as proposed by Feuillet et al. (2021) for the EMVC). The N'Droundé volcanic province is made of N160–180°E striking ridges arranged in a right-stepping échelons in an NNE-SSW direction. They likely also formed as a result of volcano-tectonic processes to accommodate this N40°E extension. Their arrangement in the echelons suggests a left lateral component of slip in the NNE-SSW direction, compatible with the N40°E striking extensional stress field. All the structures we identified in the archipelago are rifts or extensional features that accommodate a regional N40°E extension (Figure 15). No Riedel shears or compressional structures is observed in our data set. The EMVC parallels to the Jumelles-Mwezi-rift and is probably an extensional feature and not a strike-slip structure, as proposed by Famin et al. (2020).

At a larger scale (that of the entire archipelago), the Mwezi, N'Drounde rift and the "0" structure are arranged in left stepping échelons in an E-W direction (Figures 14 and 15). These extensional structures are thus the result of a N40°E extension active in an E-W strike zone about 200 km wide. This arrangement implies that the E-W zone is a right lateral shear zone. It extends between the southern tip of the EARS offshore branch and the northern part of Madagascar, where NNW-SSE to NS striking quaternary rifts (Alotra-Ankai, Antogil, Ankaratra) and volcanic complexes (Ambre, Nosy Be) accommodate an E-W extension (Figures 1 and 15, Rufer et al., 2014). The Mwezi and N'Drounde rifts are part of an E-W striking, 800 km-wide, 200 km-long transfer zone (or Rift Interaction Zone (RIZ), Kolawole & Ajala, 2024) connecting two N-S striking plate scale continental rift systems (EARS and Malagasy rift). Our result thus confirms the previous hypothesis by Feuillet et al. (2021) who inferred a transfer zone in this area. The arrangement of the Mwezi and N'Drounde rifts and other N130°E striking ridges (extensional structures) but also the presence of more easterly structures in between bear a striking resemblance to the structures promoted by analog material model of rift related transfer zones (with volcanism or not, Corti et al., 2007; Dauteuil et al., 2002, DeSouza Rodrigues, 2023). These structures are normal faults or extensional structures oblique to the main rift and arrange in echelon in a wide zone. The transfer zone is wide (more than 200 km, Figure 15), comparable to the one in the Ethiopian and the northern Kenya rift, possibly resulting from widespread intrusions at the base of the lithosphere, as inferred by Corti et al. (2022). Dauteuil et al. (2002) showed that oblique normal faults can develop in wide transfer zones when the lithosphere is weak, (above a plume for example) or/and when the offset length is small (early stage system).

The rift propagation could contribute to damage the lithosphere at the tip of the rift. The lithosphere may thus be weakened at the interacting tips of two rifts, facilitating the development of a wide transfer zone at the early stage of rift interaction, as observed elsewhere in the EARS (Ajala et al., 2024; Kolawole & Ajala, 2024). Local or regional heterogeneities, such as the presence of old crustal transform zones in the Somali Basin (Phethean et al., 2016) or variation of the basal topography of the lithosphere (Rajaonarison et al., 2020), but also the presence of magmatic reservoirs or mush zones, might control the development and the geometry of individual structures in the transfer zone as documented elsewhere in the EARS (Kolawole et al., 2021). We showed that the smaller-scale fault zones hosted in the RIZ (Mwezi and N'Drounde) are themselves propagating rifts. We showed that they are young Plio-Pleistocene and evolved by pulses. The pulses may be coeval with those along the East African and Malagasy rifts. The ages of "hosted" small rifts are coeval with the formation of the southernmost part of the EARS branch off the Mozambique coast (Franke et al., 2015). The Comoros transfer zone was formed at that time.

5.3. Possible Origin of the Volcanism

We documented a recent rift pulse that could be the only one that took place in the Mwezi-Jumelles area over the last 1 Ma. We estimated that a total volume of lava of 32 km^3 erupted during this pulse. This volume is equal to the volume of magma present in sills. This ratio between intruded and extruded volumes is 1:1, at the upper end of the range of those estimated for other regions (Kay & Kay, 1985; Lipman, 1995). This ratio is closer to 1:3 for most volcanic fields or single volcanoes (White et al., 2006). However, our estimate is subject to large uncertainties and could be lower.

The total volume of lava in Mwezi is five times larger than the volume erupted at the newly formed Fani Maore, offshore Mayotte (6 km^3) and comparable to the volume of Minoan eruption at Santorini Rift (Karstens

et al., 2023). The total volume of lava extruded in basaltic volcanic fields strongly varies (White et al., 2006) and ranges between 2 km^3 (Auckland continental volcanic field—Allen & Smith, 1994) and 125 km^3 (La Palma volcano—Carracedo et al., 1999). With approximately 32 km^3, the estimated volume for the volcanic phase in the Mwezi volcanic field is close to the total extruded volumes of the Bouvet hot-spot (28 km^3—Gerlach, 1990) or the Coso volcanic field in California (24 km^3—Duffield et al., 1980).

We showed that, apart from the lava and volcanic cones set on the border fault, the volcanic edifices observed on the seafloor of the Mwezi volcanic province were set up in the last 1 Ma. Considering a 32 km^3 of extruded volume during the unique rift pulse over the last 1 Ma, the mean eruptive flux over the last Ma in the field is 3.2×10^{-2} $km^3.ka^{-1}$. This flux is comparable to that of the Camargo volcanic field in Mexico (0.026 $km^3.ka^{-1}$, Aranda-Goméz et al., 2003) or the Eifel East volcanic field in the Rhenish Massif (0.02 $km^3.ka^{-1}$—Schmincke et al., 1983; Van den Hove et al., 2017), which are both continental rifts.

Duvernay et al. (2021), proposed that large eruptive fluxes for volcanic fields are best explained by a plume-related origin of the volcanism, while lower eruptive fluxes (<0.2 $km^3.ka^{-1}$) are indicative of an alternative magmatic alimentation process such as Edge-Driven Convection (EDC), Shear-Driven Upwelling (SDU), or both. Given the eruptive flux in the Mwezi volcanic field, the processes for melt generation would be more consistent with SDU or EDC. Rajaonarison et al. (2020) and Fishwick (2010), showed that the lithosphere beneath the North Mozambique Channel and Madagascar is thinner in the Somali Basin (80 km), and thicker in the Comoros and Mozambique Basins (110 km). According to these authors, this creates a heterogeneity at the base of the lithosphere, coinciding with the location of the Comoros archipelago. Through numerical models, Rajaonarison et al. (2020) showed that the lithospheric heterogeneity alone is sufficient to generate EDC beneath Madagascar, while in North Madagascar and the Comoros archipelago this phenomenon is also influenced by the mantellic flow of the East African superplume.

The results from our study indicate that the melt feeding the volcanism of the Mwezi province and, by extrapolating, the Comoros archipelago, may originate from Edge Driven Convective Processes. This process may operate in conjunction with large scale thermal processes due to the presence of branches of the East African superplume (Wamba et al., 2023).

6. Conclusions

From the analysis, interpretation, and detailed analysis of the geophysical data acquired in the Comoros archipelago, we identified and characterized various volcano-tectonic structures (lava flows, cones, dykes, faults, sills and forced folds) on the seafloor and in the sedimentary cover. Their distribution and organization show that they are the result of interactions between volcanism and tectonics. We showed that the great Jumelles-Mwezi and N'Drounde volcanic provinces, recently identified in the North Mozambique abyssal plain and part of the Comoros volcanism, could each represent a distinct rift system. The Jumelles-Mwezi Rift, formed 5 Ma ago and propagated Northwestwards over tens of kilometers during a major diking event less than 200 ka. From the chronology of deformed sediments, we showed that this event was brief and unique over the last 800 ka. Recent geological markers for rifting include large lava flows (which backscatter signatures indicate a northwestward propagation of the system) and the folding of the seafloor by recent volcanic intrusions. The N'Drounde rift is made of right stepping en-échelons ridges that were emplaced between ~1 and 0.5 Ma along normal faults in a N10°E direction. The N'Drounde rift is part of a larger system including the onshore volcanism of Grande-Comore (La Grille and Karthala shield volcanoes) and the Domoni submarine morphological ridge, south of the island. We propose that the main magma reservoirs or mush zones, that feed the Jumelles-Mwezi and N'Droundé rifts via dikes and sills systems in the lithosphere and the sedimentary cover, lie beneath the Jumelles seamounts and the Karthala shield volcano, respectively. On a regional scale, the rifts arrange in left-stepping échelons in a 200 km-wide, E-W trending zone, between the offshore branch of the EARS and the Malagasy rifts. They open up and evolve to accommodate a NE-SW regional extension resulting from east-west dextral shearing in a Rift Interaction Zone (RIZ or transfer zone). We calculated that 32 km^3 of lava emplaced in the Mwezi area in the late Quaternary. These volumes and flux are small compared to what is expected in volcanic zone fed by deep mantle plumes. This suggests that the volcanism may also originate from more shallower processes, such as edge-driven convection or shear-driven upwelling promoted by extensional tectonics.

Data Availability Statement

For the processed data & analyses, the storage is in progress (available at the end of the research project (end of 2025). From Data management plan of the COYOTES project, the processed data & analyses will be stored in the national database (BSSmer, BGMg) retrievable on the InfoTerre (https://infoterre.brgm.fr/) and/or Seadatanet websites (https://www.seadatanet.org/). Concerning the raw data, some are already in open access (ref: https://doi.org/10.17600/18001331). It is managed by SISMER and available at https://campagnes.flotteoceanographique.fr/campagnes/18001331/.

Acknowledgments
The SISMAORE campaign was mainly funded by the Flotte Océanographique Française (FOF) and the French geological survey (BRGM). We thank the crew of the research vessel Pourquoi Pas and technicians of GENAVIR team for the bathymetry processing and the seismic deployment. We particularly thank the scientific team for the acquisition and onboard seismic processing. This study was supported and financed by the French National Research Agency (ANR) in the framework of the COYOTES project (COmores & maYotte: vOlcanisme, TEctonique et Sismicité; ANR-19-CE31-0018; https://anr.fr/Projet-ANR-19-CE31-0018). We are grateful to the French National Marine Hydrographic and Oceanographic Service (SHOM), the SCRATCH team and REVOSIMA for providing additional bathymetric data of the area. We are also thankful to the members of the SISMAORE and COYOTES teams for the insightful discussions. Particularly, we would like to thank C. Masquelet and A. Rusquet for sharing their results of works on the Comoros archipelago.

References

Acocella, V. (2021). Volcano-tectonic processes. In *Advances in volcanology*. Springer International Publishing. https://doi.org/10.1007/978-3-030-65968-4

Acocella, V., Morvillo, P., & Funiciello, R. (2005). What controls relay ramps and transfer faults within rift zones? Insights from analogue models. *Journal of Structural Geology*, *27*(3), 397–408. https://doi.org/10.1016/j.jsg.2004.11.006

Acocella, V., & Neri, M. (2009). Dike propagation in volcanic edifices: Overview and possible developments. *Tectonophysics*, *471*(1–2), 67–77. https://doi.org/10.1016/j.tecto.2008.10.002

Ajala, R., Kolawole, F., & Menke, W. (2024). Blind magmatism abets nonvolcanic continental rifting. *Communications Earth & Environment*, *5*(1), 80. https://doi.org/10.1038/s43247-024-01244-7

Allen, S., & Smith, I. (1994). *Eruption styles and voIcanic hazardin the AuckIand voIcanic field New ZeaJand*. Shizuoka University REpository. s. d.

Aranda-Gómez, J. J., Luhr, J. F., Housh, T. B., Connor, C. B., Becker, T., & Henry, C. D. (2003). Synextensional Pliocene–Pleistocene eruptive activity in the Camargo volcanic field, Chihuahua, México. *Geological Society of America Bulletin*, *115*, 298–313. https://doi.org/10.1130/0016-7606(2003)115<0298:SPPEAI>2.0.CO;2

Audru, J.-C., Guennoc, P., Thinon, I., & Abellard, O. (2006). Bathymay: la structure sous-marine de Mayotte révélée par l'imagerie multi-faisceaux. *Comptes Rendus Geoscience*, *338*(16), 1240–1249. https://doi.org/10.1016/j.crte.2006.07.010

Augustin, J. M. (1997). Applications of an image segmentati technique to multibeam echo-sounde.

Augustin, J. M., Le Suave, R., Lurton, X., Voisset, M., Dugelay, S., & Satra, C. (1996). Contribution of the multibeam acoustic imagery to the exploration of the sea-bottom: Examples of SOPACMAPS 3 and ZoNéCo 1 cruises. *Marine Geophysical Researches*, *18*(2–4), 459–486. https://doi.org/10.1007/BF00286090

Bachèlery, P. (1995). L'éruption phréatique du Karthala (Grande Comore) en Juillet 1991. *Comptes rendus de l'Académie des sciences. Série 2. Sciences de la terre et des planètes* (Vol. 320, pp. 691–698).

Bachèlery, P., Lenat, J.-F., Di Muro, A., & Michon, L. (2016). *Active volcanoes of the southwest Indian Ocean: Piton de La Fournaise and Karthala*. Active Volcanoes of the World. https://doi.org/10.1007/978-3-642-31395-0

Bachèlery, P., Morin, J., Villeneuve, N., Soulé, H., Nassor, H., & Ali, A. R. (2016). Structure and eruptive history of Karthala volcano. In P. Bachèlery, J.-F. Lenat, A.D. Muro, & L. Michon (Eds.), *Active volcanoes of the southwest Indian Ocean*, (pp. 345–366). Active Volcanoes of the World. Springer Berlin Heidelberg. https://doi.org/10.1007/978-3-642-31395-0_22

Berthod, C., Médard, E., Bachèlery, P., Gurioli, L., Di Muro, A., Peltier, A., et al. (2021). The 2018-ongoing Mayotte submarine eruption: Magma migration imaged by petrological monitoring. *Earth and Planetary Science Letters*, *571*, 117085. https://doi.org/10.1016/j.epsl.2021.117085

Bertil, D., Mercury, N., Doubre, C., Lemoine, A., & Woerd, J. V. D. (2022). The unexpected Mayotte 2018–2020 seismic sequence: A reappraisal of the regional seismicity of the Comoros. *Comptes Rendus Geoscience*, *353*(S1), 211–235. https://doi.org/10.5802/crgeos.79

Bertil, D., & Regnoult, J. M. (1998). Seismotectonics of Madagascar. *Tectonophysics*, *294*(1–2), 57–74. https://doi.org/10.1016/S0040-1951(98)00088-2

Bésairie, H. (1957). Carte Tectonique de Madagascar—Echelle 1/2500000. In *Service Géologique et Société des Pétroles de Madagasacar*. Bibliothèque du Museum d'Histoire Naturelle.

Bischoff, A. P., Nicol, A., & Beggs, M. (2017). Stratigraphy of architectural elements in a buried volcanic system and implications for hydrocarbon exploration. *Interpretation*, *5*(3), SK141–SK159. https://doi.org/10.1190/INT-2016-0201.1

Bordenca, C. V. F., Caracausi, B., Coltorti, A., Di Muro, M., Pik, A., Rizzo, R., et al. (2023). The nature of the mantle beneath La Grille volcano (Grande Comore Island, Western Indian Ocean) as revealed by mineral chemistry, noble gas geochemistry, CO_2 abundance and radiogenic isotopes of ultramafic mantle xenoliths. *Lithos*, *462–463*, 107406. https://doi.org/10.1016/j.lithos.2023.107406

Bosworth, W., Stockli, D. F., & Helgeson, D. E. (2015). Integrated outcrop, 3D seismic, and geochronologic interpretation of red sea dike-related deformation in the western desert, Egypt—The role of the 23Ma Cairo "Mini-plume". *Journal of African Earth Sciences*, *109*, 107–119. https://doi.org/10.1016/j.jafrearsci.2015.05.005

Cailleau, B., Walter, T. R., Janle, P., & Ernst, H. (2003). Modeling volcanic deformation in a regional stress field: Implications for the formation of Graben structures on Alba Patera, Mars: Deformation of Alba Patera volcano, Mars. *Journal of Geophysical Research*, *108*(E12), 5141. https://doi.org/10.1029/2003JE002135

Calais, E., Ebinger, C., Hartnady, C., & Nocquet, J. M. (2006). Kinematics of the East African rift from GPS and earthquake slip vector data. *Geological Society, London, Special Publications*, *259*(1), 9–22. https://doi.org/10.1144/GSL.SP.2006.259.01.03

Carracedo, J. C., Day, S. J., Guillou, H., & Gravestock, P. (1999). Later stages of volcanic evolution of La Palma, Canary Islands: Rift Evolution, Giant Landslides, and the Genesis of the Caldera de Taburiente. *Geological Society of America Bulletin*, *111*(5), 755–768. https://doi.org/10.1130/0016-7606(1999)111<0755:LSOVEO>2.3.CO;2

Chadwick, W. W., & Howard, K. A. (1991). The pattern of circumferential and radial eruptive fissures on the volcanoes of Fernandina and Isabela Islands, Galapagos. *Bulletin of Volcanology*, *53*(4), 259–275. https://doi.org/10.1007/BF00414523

Chauvel, C. I., Gutierrez, E. C., Luu, P., Burckel, T.-H., & Pascale, P. B. (2024). Fani Maoré, a new "young HIMU" volcanoc with extreme geochemistry. *Earth and Planetary Science Letters*, *626*, 118529. https://doi.org/10.1016/j.epsl.2023.118529

Corti, G. (2012). Evolution and characteristics of continental rifting: Analog modeling-inspired view and comparison with examples from the East African Rift System. *Tectonophysics*, *522–523*, 1–33. https://doi.org/10.1016/j.tecto.2011.06.010

Corti, G., Maestrelli, D., & Federico, S. (2022). Large-to local-scale control of pre-existing structures on continental rifting: Examples from the main Ethiopian Rift, East Africa. *Frontiers in Earth Science*, *10*, 808503. https://doi.org/10.3389/feart.2022.808503

Corti, G., Van Wijk, J., Cloetingh, S., & Morley, C. K. (2007). Tectonic inheritance and continental rift architecture: Numerical and analogue models of the East African Rift System. *Tectonics*, *26*(6), 2006TC002086. https://doi.org/10.1029/2006TC002086
Courgeon, S., Bachèlery, P., Jouet, G., Jorry, S. J., Bou, E., BouDagher-Fadel, M. K., et al. (2018). The offshore East African Rift System: New insights from the Sakalaves Seamounts (Davie Ridge, SW Indian Ocean). *Terra Nova*, *30*(5), 380–388. https://doi.org/10.1111/ter.12353
Dauteuil, O., Bourgeois, O., & Mauduit, T. (2002). Lithosphere strength controls oceanic transform zone structure: Insights from analogue models. *Geophysical Journal International*, *150*(3), 706–714. https://doi.org/10.1046/j.1365-246X.2002.01736.x
Davies, R. J., & Stewart, S. A. (2005). Emplacement of giant mud volcanoes in the South Caspian Basin: 3D seismic reflection imaging of their root zones. *Journal of the Geological Society*, *162*(1), 1–4. https://doi.org/10.1144/0016-764904-082
Davis, J. K., Lawver, L. A., Norton, I. O., & Gahagan, L. M. (2016). New Somali basin magnetic anomalies and a plate model for the early Indian Ocean. *Gondwana Research*, *34*, 16–28. https://doi.org/10.1016/j.gr.2016.02.010
Desgrolard, F. (1996). Pétrologie des laves d'un volcan intraplaque océanique: Le Karthala, île de la Grande-Comore (R.F.I. des Comores). *Volcanologie. Université Joseph-Fourier—Grenoble I*, Français. ⟨NNT : ⟩. ⟨tel-00756691⟩.
De Souza Rodrigues, R., Fernando César Alves da Silva, & Barbosa Venâncio (2023). Oblique rifting along transfer zones: The structural evolution model revealed by physical modeling. *Journal of South American Earth Sciences*.
Dietterich, H. R., Diefenbach, A. K., Soule, S. A., Zoeller, M. H., Patrick, M. P., Major, J. J., & Lundgren, P. R. (2021). Lava effusion rate evolution and erupted volume during the 2018 Kīlauea lower East Rift Zone eruption. *Bulletin of Volcanology*, *83*(4), 25. https://doi.org/10.1007/s00445-021-01443-6
Duffield, W. A., Bacon, C. R., & Brent Dalrymple, G. (1980). Late Cenozoic volcanism, geochronology, and structure of the Coso Range, Inyo County, California. *Journal of Geophysical Research*, *85*(B5), 2381–2404. https://doi.org/10.1029/JB085iB05p02381
Dugelay, S., Graffigne, C., & Augustin, J. M. (1996). *Deep seafloor characterization with multibeam echosounders by image segmentation using angular acoustic variations*. In E. R. Dougherty, F. J. Preteux, & J. L. Davidson (Eds.), (pp. 255–266). https://doi.org/10.1117/12.253450
Duvernay, T., Rhodri Davies, D., Mathews, C. R., Gibson, A. H., & Kramer, S. C. (2021). Linking intraplate volcanism to lithospheric structure and asthenospheric flow. *Geochemistry, Geophysics, Geosystems*, *22*(8), e2021GC009953. https://doi.org/10.1029/2021GC009953
Ebinger, C., Ayele, A., Keir, D., Rowland, J., Yirgu, G., Wright, T., et al. (2010). Length and timescales of rift faulting and magma intrusion: The Afar rifting cycle from 2005 to present. *Annual Review of Earth and Planetary Sciences*, *38*(1), 439–466. https://doi.org/10.1146/annurev-earth-040809-152333
Ekström, G., Nettles, M., & Dziewoński, A. M. (2012). The global CMT project 2004–2010: Centroid-moment tensors for 13,017 earthquakes. *Physics of the Earth and Planetary Interiors*, *200–201*, 1–9. https://doi.org/10.1016/j.pepi.2012.04.002
Emerick, C. M., & Duncan, R. A. (1982). Age progressive volcanism in the Comores archipelago, western Indian Ocean and implications for Somali plate tectonics. *Earth and Planetary Science Letters*, *60*(3), 415–428. https://doi.org/10.1016/0012-821X(82)90077-2
Famin, V., Laurent, M., & Bourhane, A. (2020). The Comoros archipelago: A right-lateral transform boundary between the Somalia and Lwandle Plates. *Tectonophysics*, *789*, 228539. https://doi.org/10.1016/j.tecto.2020.228539
Feuillet, N., Jorry, S., Crawford, W. C., Deplus, C., Thinon, I., Jacques, E., et al. (2021). Birth of a large volcanic edifice offshore Mayotte via lithosphere-scale dyke intrusion. *Nature Geoscience*, *26*(10), 787–795. https://doi.org/10.1038/s41561-021-00809-x
Feuillet, N., Nostro, C., Chiarabba, C., & Cocco, M. (2004). Coupling between earthquake swarms and volcanic unrest at the Alban Hills volcano (Central Italy) modeled through elastic stress transfer. *Journal of Geophysical Research*, *109*(B2), 2003JB002419. https://doi.org/10.1029/2003JB002419
Fishwick, S. (2010). Surface wave tomography: Imaging of the lithosphere–Asthenosphere boundary beneath central and southern Africa? *Lithos*, *120*(1–2), 63–73. https://doi.org/10.1016/j.lithos.2010.05.011
Franke, D., Jokat, W., Ladage, S., Stollhofen, H., Klimke, J., Lutz, R., et al. (2015). The offshore East African Rift System: Structural framework at the Toe of a Juvenile Rift: The offshore East African rift. *Tectonics*, *34*(10), 2086–2104. https://doi.org/10.1002/2015TC003922
Gerlach, D. C. (1990). Eruption rates and isotopic systematics of ocean islands: Further evidence for small-scale heterogeneity in the upper mantle. *Tectonophysics*, *172*(3–4), 273–289. https://doi.org/10.1016/0040-1951(90)90035-7
Giba, M., Walsh, J. J., Nicol, A., Mouslopoulou, V., & Seebeck, H. (2013). Investigation of the spatio-temporal relationship between normal faulting and arc volcanism on million-year time scales. *Journal of the Geological Society*, *170*(6), 951–962. https://doi.org/10.1144/jgs2012-121
Gibbons, A. D., Whittaker, J. M., & Dietmar Müller, R. (2013). The breakup of East Gondwana: Assimilating constraints from Cretaceous Ocean basins around India into a best-fit tectonic model. *Journal of Geophysical Research: Solid Earth*, *118*(3), 808–822. https://doi.org/10.1002/jgrb.50079
Gonidec, Y. L., Lamarche, G., & Wright, I. C. (2003). Inhomogeneous substrate analysis using EM300 backscatter imagery. *Marine Geophysical Researches*, *24*(3–4), 311–327. https://doi.org/10.1007/s11001-004-1945-9
Grandin, R., Socquet, A., Binet, R., Klinger, Y., Jacques, E., de Chabalier, J., et al. (2009). September 2005 Manda Hararo-Dabbahu rifting event, Afar (Ethiopia): Constraints provided by geodetic data. *Journal of Geophysical Research*, *114*(B8), B08404. https://doi.org/10.1029/2008jb005843
Hamling, I. J., Ayele, A., Bennati, L., Calais, E., Ebinger, C. J., Keir, D., et al. (2009). Geodetic observations of the ongoing Dabbahu rifting episode: New dyke intrusions in 2006 and 2007. *Geophysical Journal International*, *178*(2), 989–1003. https://doi.org/10.1111/j.1365-246X.2009.04163.x
Hoek, J. D. (1995). Continental Mafic dyke swarms as tectonic indicators: An example from the Vestfold Hills, East Antarctica. *Precambrian Research*, *75*(3–4), 121–139. https://doi.org/10.1016/0301-9268(95)80002-y
Hübscher, C., Ruhnau, M., & Nomikou, P. (2015). Volcano-tectonic evolution of the polygenetic Kolumbo submarine Volcano/Santorini (Aegean Sea). *Journal of Volcanology and Geothermal Research*, *291*, 101–111. https://doi.org/10.1016/j.jvolgeores.2014.12.020
Infante-Paez, L., & Marfurt, K. J. (2017). Seismic expression and geomorphology of igneous bodies: A Taranaki Basin, New Zealand, case study. *Interpretation*, *5*(3), SK121-40–SK140. https://doi.org/10.1190/INT-2016-0244.1
Jacques-André, M. (1991). Nouvelles contraintes sur la cinématique de la chaine de Madagascar: Les structures de la chaine de Davie.
Karstens, J., Preine, J., Crutchley, G. J., Kutterolf, S., Van Der Bilt, W. G. M., Hooft, E. E. E., et al. (2023). Revised Minoan eruption volume as benchmark for large volcanic eruptions. *Nature Communications*, *14*(1), 2497. https://doi.org/10.1038/s41467-023-38176-3
Kay, S. M., & Kay, R. W. (1985). Role of crystal cumulates and the oceanic crust in the formation of the lower crust of the Aleutian Arc. *Geology*, *13*(7), 461. https://doi.org/10.1130/0091-7613(1985)13<461:ROCCAT>2.0.CO;2
Kirton, S. R., & Donato, J. A. (1985). Some buried tertiary dykes of Britain and surrounding waters deduced by magnetic modelling and seismic reflection methods. *Journal of the Geological Society*, *142*(6), 1047–1057. https://doi.org/10.1144/gsjgs.142.6.1047
Klimke, J., & Franke, D. (2016). Gondwana breakup: No evidence for a Davie fracture zone offshore northern Mozambique, Tanzania and Kenya. *Terra Nova*, *28*(4), 233–244. https://doi.org/10.1111/ter.12214

Kolawole, F., & Ajala, R. (2024). Propagating rifts: The roles of crustal damage and ascending mantle fluids. *Solid Earth*, *15*(7), 747–762. https://doi.org/10.5194/se-15-747-2024

Kolawole, F., Firkins, M. C., Al Wahaibi, T. S., Atekwana, E. A., & Soreghan, M. J. (2021). Rift interaction zones and the stages of rift linkage in active segmented continental rift systems. *Basin Research*, *33*(6), 2984–3020. https://doi.org/10.1111/bre.12592

Krafft, M. (1982). Comptes rendus des séances de l'Académie des sciences. Série 2, Mécanique-physique, Chimie. *Sciences de l'univers, Sciences de la Terre*. s. d.

Kusky, T. M., Toraman, E., Raharimahefa, T., & Christine, R. (2010). Active tectonics of the Alaotra–Ankay Graben system, Madagascar: Possible extension of Somalian–African diffusive plate boundary? *Gondwana Research*, *18*(2–3), 274–294. https://doi.org/10.1016/j.gr.2010.02.003

LANCELOT Yves. (1996). MOZAPHARE-MD104 cruise. *RV Marion Dufresne*. https://doi.org/10.17600/96200060

Lawyer, L. A., Gahagan, L. M., & Ian, W. D. D. (1991). A tight fit-early Mesozoic Gondwana, a plate reconstruction perspective. *16*.

Lemoine, A., Briole, P., Bertil, D., Roullé, A., Foumelis, M., Thinon, I., et al. (2020). The 2018–2019 seismo-volcanic crisis East of Mayotte, Comoros Islands: Seismicity and ground deformation markers of an exceptional submarine eruption. *Geophysical Journal International*, *223*(1), 22–44. https://doi.org/10.1093/gji/ggaa273

Lipman, P. W. (1995). Declining growth of Mauna Loa during the last 100,000 years: Rates of lava accumulation vs. Gravitational subsidence. In J. M. Rhodes, & J. P. Lockwood, (Eds.), *Geophysical monograph series* (Vol. 92, pp. 45–80). American Geophysical Union. https://doi.org/10.1029/GM092p0045

Lurton, X. (2002). *An introduction to underwater acoustics*. Institut de Recherche pour l'Exploitation de la Mer (IFREMER): Springer-Praxis books in Geophysical Sciences.

Magee, C., Hunt-Stewart, E., & Jackson, C. A.-L. (2013). Volcano growth mechanisms and the role of sub-volcanic intrusions: Insights from 2D seismic reflection data. *Earth and Planetary Science Letters*, *373*, 41–53. https://doi.org/10.1016/j.epsl.2013.04.041

Magee, C., & Jackson, C. A.-L. (2020). Seismic reflection data reveal the 3D structure of the newly discovered exmouth dyke swarm, offshore NW Australia. *Solid Earth*, *11*(2), 579–606. https://doi.org/10.5194/se-11-579-2020

Magee, C., Muirhead, J. D., Karvelas, A., Holford, S. P., Jackson, C. A. L., Bastow, I. D., et al. (2016). Lateral magma flow in Mafic sill complexes. *Geosphere*, *12*(3), 809–841. https://doi.org/10.1130/GES01256.1

Masquelet, C., Leroy, S., Delescluse, M., Chamot-Rooke, N., Thinon, I., Lemoine, A., et al. (2022). The East-Mayotte new volcano in the Comoros archipelago: Structure and timing of magmatic phases inferred from seismic reflection data. *Comptes Rendus Geoscience*, *354*(S2), 1–15. https://doi.org/10.5802/crgeos.154

Masquelet, C., Leroy, S., Sauter, D., Chamot-Rooke, N., & Thinon, I. (2023). Magmatisme, héritage et déformation autour de l'archipel des Comores, dans le bassin de Somalie. Implications géodynamiques (Thèse de doctorat). Thèses.fr. 2023SORUS613 http://www.theses.fr/2023SORUS613

Medialdea, T., Somoza, L., González, F. J., Vázquez, J. T., de Ignacio, C., Sumino, H., et al. (2017). Evidence of a modern deep water magmatic hydrothermal system in the canary basin (eastern central Atlantic Ocean). *Geochemistry, Geophysics, Geosystems*, *18*(8), 3138–3164. https://doi.org/10.1002/2017GC006889

Michon, L. (2016). The volcanism of the Comoros archipelago integrated at a regional scale. In P. Bachelery, J.-F. Lenat, A.D. Muro, & L. Michon, (Eds.), *Active volcanoes of the southwest Indian Ocean* (pp. 333–344). Active Volcanoes of the World, Springer Berlin Heidelberg. https://doi.org/10.1007/978-3-642-31395-0_21

Michon, L., Vincent, F., & Xavier, Q. (2022). Evolution of the East African Rift System from trap-scale to plate-scale rifting. *Earth-Science Reviews*, *231*, 104089. https://doi.org/10.1016/j.earscirev.2022.104089

Mitchell, N. C. (1993). A model for attenuation of backscatter due to sediment accumulations and its application to determine sediment thicknesses with GLORIA Sidescan Sonar. *Journal of Geophysical Research*, *98*(B12), 22477–22493. https://doi.org/10.1029/93JB02217

Mitchum, R. M., Vail, P. R., & Thompson, S. (1977). Seismic stratigraphy and global changes of sea level, Part 2. The depositional sequence as a basic unit for stratigraphic Analysis[1]. In C. E. Payton (Ed.), *Seismic stratigraphy—Applications to hydrocarbon exploration*, American Association of Petroleum Geologists. https://doi.org/10.1306/M26490C4

Mougenot, D., Recq, M., Virlogeux, P., & Lepvrier, C. (1986). Seaward extension of the East African Rift. *Nature*, *321*(6070), 599–603. https://doi.org/10.1038/321599a0

Muller. (1977). The stress state near Spanish Peaks, Colorado determined from a dike pattern. 115

Nelson, R. A., Patton, T. L., & Morley, C. K. (1992). Rift-segment interaction and its relation to hydrocarbon exploration in continental rift systems (1). *AAPG Bulletin*, *76*(8), 1153–1169. https://doi.org/10.1306/bdff898e-1718-11d7-8645000102c1865d

Nougier, J., Cantagrel, J. M., & Karche, J. P. (1986). The Comores archipelago in the western Indian Ocean: Volcanology, geochronology and geodynamic setting. *Journal of African Earth Sciences*, *5*(2), 135–145. https://doi.org/10.1016/0899-5362(86)90003-5

Odé, H. (1957). *Mechanical analysis of the dyke pattern of the Spanish peaks area, Colorado*. Bulletin of the Geophysical Society of America.

Paquet, F., Dauteuil, O., Hallot, E., & Moreau, F. (2007). Tectonics and magma dynamics coupling in a dyke swarm of Iceland. *Journal of Structural Geology*, *29*(9), 1477–1493. https://doi.org/10.1016/j.jsg.2007.06.001

Perrin, C., Manighetti, I., Ampuero, J.-P., Cappa, F., & Gaudemer, Y. (2016). Location of largest earthquake slip and fast rupture controlled by along-strike change in fault structural maturity due to fault growth. *Journal of Geophysical Research: Solid Earth*, *121*(5), 3666–3685. https://doi.org/10.1002/2015JB012671

Phethean, J. J. J., Kalnins, L. M., van Hunen, J., Biffi, P. G., Davies, R. J., & McCaffrey, K. J. W. (2016). Madagascar's escape from Africa: A high-resolution plate reconstruction for the western Somali Basin and implications for supercontinent dispersal: Madagascar'S escape from Africa. *Geochemistry, Geophysics, Geosystems*, *17*(12), 5036–5055. https://doi.org/10.1002/2016GC006624

Piqué, A., Laville, E., Chotin, P., Chorowicz, J., Rakotondraompiana, S., & Thouin, C. (1999). L'extension à Madagascar du Néogène à l'Actuel: arguments structuraux et géophysiques. *Journal of African Earth Sciences*, *28*(4), 975–983. https://doi.org/10.1016/S0899-5362(99)00073-1

Preine, J., Hübscher, C., Karstens, J., & Nomikou, P. (2022). Volcano-tectonic evolution of the Christiana-SantoriniKolumbo rift zone. *Tectonics*, *41*(11). https://doi.org/10.1029/2022tc007524

Preine, J., Karstens, J., Hübscher, C., Crutchley, G. J., Druitt, T. H., Schmid, F., & Nomikou, P. (2022). The hidden giant: How a rift pulse triggered a cascade of sector collapses and voluminous secondary mass-transport events in the early evolution of Santorini. *Basin Research*, *34*(4), 1465–1485. https://doi.org/10.1111/bre.12667

Priyadarshi, C. K., Niyazi, Y., Eruteya, O. E., Moscariello, A., Mark, W., Ierodiaconou, D., & Sain, K. (2022). Anatomy of intrusion related forced fold in the offshore Otway Basin, SE Australia. *Marine and Petroleum Geology*, *141*, 105719. https://doi.org/10.1016/j.marpetgeo.2022.105719

Quidelleur, X., Laurent, M., Vincent, F., Geffray, M.-C., Danišík, M., Gardiner, N., et al. (2022). Holocene volcanic activity in Anjouan Island (Comoros archipelago) revealed by new Cassignol-Gillot groundmass K–Ar and 14C ages. *Quaternary Geochronology*, *67*, 101236. https://doi.org/10.1016/j.quageo.2021.101236

Rajaonarison, T. A., Stamps, D. S., Fishwick, S., Brune, S., Glerum, A., & Hu, J. (2020). Numerical modeling of mantle flow beneath Madagascar to constrain upper mantle rheology beneath continental regions. *Journal of Geophysical Research: Solid Earth*, *125*(2), e2019JB018560. https://doi.org/10.1029/2019JB018560

Rinnert, E., Cathalot, C., & Feuillet, N. (2021). GEOFLAMME cruise, RV Pourquoi pas? https://doi.org/10.17600/18001297

Rinnert, E., Lebas, E., Komorowski, J.-C., Paquet, F., Jorry, S., Feuillet, N., et al. (2019). MAYOBS. https://doi.org/10.18142/291

Rufer, D., Preusser, F., Schreurs, G., Gnos, E., & Berger, A. (2014). Late Quaternary history of the Vakinankaratra volcanic field (central Madagascar): Insights from luminescence dating of phreatomagmatic eruption deposits. *Bulletin of Volcanology*, *76*, 817. https://doi.org/10.1007/s00445-014-0817-7

Rusquet, A., Famin, V., Michon, L., Quidelleur, X., Nauret, F., Danišík, M., et al. (2025). Phases of magmatism and tectonics along the Madagascar-Comoros Volcanic chain, and synchronous changes in the kinematics of the Lwandle and Somalia plates. *Journal of Geophysical Research: Solid Earth*, *130*(1), e2024JB029488. https://doi.org/10.1029/2024JB029488

Rusquet, A., Vincent, F., Quidelleur, X., Michon, L., Nauret, F., Danišík, M., et al. (2023). Pliocene-to-Holocene volcano-tectonic activity on Mohéli Island (Comoros Archipelago) constrained by new K Ar ages. *Journal of Volcanology and Geothermal Research*, *442*, 107896. https://doi.org/10.1016/j.jvolgeores.2023.107896

Saria, E., Calais, E., Stamps, D. S., Delvaux, D., & Hartnady, C. J. H. (2014). Present-day kinematics of the East African Rift. *Journal of Geophysical Research: Solid Earth*, *119*(4), 3584–3600. https://doi.org/10.1002/2013JB010901

Schmincke, H.-U., Lorenz, V., & Seck, H. A. (1983). The quaternary Eifel volcanic fields. In K. Fuchs, K. V. Gehlen, H. Mälzer, H. Murawski, & A. Semmel (Eds.), *Plateau uplift* (pp. 139–151). Springer Berlin Heidelberg. https://doi.org/10.1007/978-3-642-69219-2_21

Shom. (2016). Projet Homonim. https://doi.org/10.17183/MNT_MAY100m_HOMONIM_WGS84

Shoulders, S. J., & Cartwright, J. (2004). Constraining the depth and timing of large-scale conical sandstone intrusions. *Geology*, *32*(8), 661. https://doi.org/10.1130/G20654.1

Sigmundsson, F., Hooper, A., Hreinsdóttir, S., Vogfjörd, K. S., Ófeigsson, B. G., Heimisson, E. R., et al. (2015). Segmented lateral dyke growth in a rifting event at Bárðarbunga volcanic system, Iceland. *Nature*, *517*(7533), 191–195. https://doi.org/10.1038/nature14111

Srivastava, R. K., Ernst, R. E., & Peng, P. (2019). Dyke swarms of the world: A modern perspective. In *Springer geology*. Springer Singapore. https://doi.org/10.1007/978-981-13-1666-1

Stamps, D. S., Kreemer, C., Fernandes, R., Rajaonarison, T. A., & Rambolamanana, G. (2021). Redefining East African Rift System kinematics. *Geology*, *49*(2), 150–155. https://doi.org/10.1130/G47985.1

Stamps, D. S., Saria, E., & Kreemer, C. (2018). A geodetic strain rate model for the East African Rift System. *Scientific Reports*, *8*(1), 732. https://doi.org/10.1038/s41598-017-19097-w

Stearns, D. (1978). "Faulting and forced folding in the Rocky Mountains foreland", Laramide folding associated with basement block faulting in the western United States, Vincent Matthews, III.

Thinon, I., Lemoine, A., & Leroy, S. (2020). Discovery of recent volcanic and tectonic provinces along the Comoros archipelago (North Mozambique channel)—Preliminary results of the SISMAORE oceanographic cruise (ANR-COYOTES project).

Thinon, I., Lemoine, A., Leroy, S., Paquet, F., Berthod, C., Zaragosi, S., et al. (2022). Volcanisme et Tectonique Découverts Le Long de l'archipel Des Comores Entre l'Afrique et Madagascar. *Comptes Rendus Geoscience*, *354*(S2), 7–34. https://doi.org/10.5802/crgeos.159-fr

Thomson, K., & Hutton, D. (2004). Geometry and growth of sill complexes: Insights using 3D seismic from the North rockall trough. *Bulletin of Volcanology*, *66*(4), 364–375. https://doi.org/10.1007/s00445-003-0320-z

Trude, J., Cartwright, J., Davies, R. J., & Smallwood, J. (2003). New technique for dating Igneous sills. *Geology*, *31*(9), 813. https://doi.org/10.1130/G19559.1

Tzevahirtzian, A., Zaragosi, S., Bachèlery, P., Biscara, L., & Marchès, E. (2021). Submarine morphology of the Comoros volcanic archipelago. *Marine Geology*, *432*, 106383. https://doi.org/10.1016/j.margeo.2020.106383

Urick, R. J. (1983). Principles of underwater sound.

Van Den Hove, J. C., Van Otterloo, J., Betts, P. G., Ailleres, L., & Cas, R. A. F. (2017). Controls on volcanism at intraplate basaltic volcanic fields. *Earth and Planetary Science Letters*, *459*, 36–47. https://doi.org/10.1016/j.epsl.2016.11.008

Wall, M., Cartwright, J., Davies, R., & McGrandle, A. (2010). 3D seismic imaging of a tertiary dyke swarm in the southern North Sea, UK. *Basin Research*, *22*(2), 181–194. https://doi.org/10.1111/j.1365-2117.2009.00416.x

Wamba, D., Jean-Paul Montagner, M., & Barbara, R. (2023). Imaging deep-mantle plumbing beneath La Réunion and Comores hot spots: Vertical plume conduits and horizontal ponding zones. *Science Advances*, *9*(4), eade3723. https://doi.org/10.1126/sciadv.ade3723

White, S., Crisp, J., & Frank, S. (2006). Long-term volumetric eruption rates and magma budgets. *Geochemistry, Geophysics, Geosystems*, *7*(3), Q03010. https://doi.org/10.1029/2005gc001002

Wright, I. C., Parson, L. M., & Gamble, J. A. (1996). Evolution and interaction of migrating cross-arc volcanism and backarc rifting: An example from the southern Havre trough (35°20′–37°S). *Journal of Geophysical Research*, *101*(B10), 22071–22086. https://doi.org/10.1029/96JB01761

Wright, T. J., Ebinger, C., Biggs, J., Ayele, A., Yirgu, G., Keir, D., & Anna, S. (2006). Magma-maintained rift segmentation at continental rupture in the 2005 Afar dyking episode. *Nature*, *442*(7100), 291–294. https://doi.org/10.1038/nature04978

Zinke, J., Reijmer, J., & Thomassin, B. (2003). Systems tracts sedimentology in the lagoon of Mayotte associated with the Holocene transgression. *Sedimentary Geology*, *160*(1–3), 57–79. https://doi.org/10.1002/jgrb.50079